Generalized plasma waves in layered superconductors: A unified approach

F. Gabriele, C. Castellani, and L. Benfatto*
Department of Physics and ISC-CNR, Sapienza, University of Rome, P.le A. Moro 5, 00185 Rome, Italy

(Received 25 October 2021; revised 1 April 2022; accepted 6 April 2022; published 11 May 2022)

In a layered and strongly anisotropic superconductor, the hybrid modes provided by the propagation of electromagnetic waves in the matter identify two well-separated energy scales connected to the large in-plane plasma frequency and to the soft out-of-plane Josephson plasmon. Despite wide interest in their detection and manipulation by means of different experimental protocols, the physical ingredients underlying a unified description of plasma waves valid at arbitrary energy and momentum are still poorly understood. Here we provide a complete description of generalized plasma waves in layered superconductors in terms of the gauge-invariant superconducting phase by including both the Coulomb interaction and the relativistic effects. We show that the anisotropy of the superfluid response leads to two intertwined hybrid light-matter modes with mixed longitudinal and transverse character, while a purely longitudinal plasmon is only recovered for wave vectors larger than the crossover scale set in by the plasma-frequency anisotropy. Interestingly, below such scale both modes appear with equal weight in the physical density response. Our results open a promising perspective for plasmonic applications made possible by next-generation spectroscopic techniques able to combine submicron momentum resolution with THz energy resolution.

DOI: 10.1103/PhysRevResearch.4.023112

I. INTRODUCTION

Plasmons represent the fundamental excitations of the conduction electrons in metals, and their existence can be easily understood within a classical framework based on Maxwell's equations. Indeed, in a source-free metal, bulk plasmons are characterized by zero magnetic field and longitudinal electric field ($\nabla \times \mathbf{E} = 0$), so they trivially satisfy Maxwell's equations under the condition of vanishing permittivity [1]. Since the longitudinal electric field couples to density fluctuations, the plasma excitation also appears in the charge-density response as a collective mode of the electron gas [2,3]. Such a hybrid light-matter mode is the longitudinal counterpart of the so-called transverse plasma polariton. Polaritons in layered two-dimensional materials and interfaces have attracted a lot of attention [4], since the spatial confinement at the interface between a thin metallic film and a dielectric gives rise to propagating modes that can be launched and visualized by using near-field optical microscopy [5]. When the metal undergoes a superconducting (SC) transition, plasmons also characterize the fluctuation spectrum of the SC phase of the complex order parameter formed below the SC critical temperature T_c [6]. Indeed, as originally pointed out by Anderson [7], the soundlike propagating phase mode of the neutral superfluid [2] is converted into gapped plasma oscillations in a charged superconductor. The appearance of the plasma mode in the spectrum of phase fluctuations is a natural consequence of the fact that the quantum phase of electrons is the variable conjugate to the density [6–9]. From a theoretical point of view, such an equivalence has been often exploited in the literature to determine the plasma dispersion of a superconductor via the study of the spectrum of the phase mode. The latter can be carried out in a rather elegant and compact way by directly deriving the quantum action for the phase degrees of freedom [6,8–13], as we will discuss in detail in this paper.

From an experimental point view, there is a strong interest in materials hosting stacks of SC sheets with weak interlayer SC Josephson coupling [14,15]. For the sake of concreteness, we will model them as xy SC planes stacked along the z direction, see Fig. 1(a). The benchmark example of such a system is provided by high-temperature cuprate superconductors [16]. The direct consequence of the weak interlayer coupling is that the plasma energy ω_z associated with phase (or density) fluctuations among the planes is substantially smaller than the one, ω_{xy}, connected with in-plane fluctuations. In the SC state, an indirect evidence of this is the large anisotropy of the in-plane versus out-of-plane penetration depths [17–19], given by $\lambda_{xy/z} = c/\omega_{xy/z}$. Since the SC gap opening below T_c suppresses particle-hole excitations, the low-energy out-of-plane Josephson plasmon becomes undamped, and was observed long ago via reflectivity measurements as a clear plasma edge emerging below T_c at few THz in several cuprates [20–24]. At finite momentum, the dispersion of the Josephson plasmon has been derived by linearizing the sine-Gordon equations for the phase difference among the planes [14,15,25–29], leading to

$$\omega_p^2(\mathbf{k}) = \omega_z^2\left(1 + \frac{c^2\gamma^2 k_{xy}^2}{\omega_{xy}^2 + c^2 k_z^2}\right), \tag{1}$$

where c is the light velocity, $\gamma = \omega_{xy}/\omega_z$ denotes the plasma-frequency anisotropy that can be up to two orders of

*lara.benfatto@roma1.infn.it

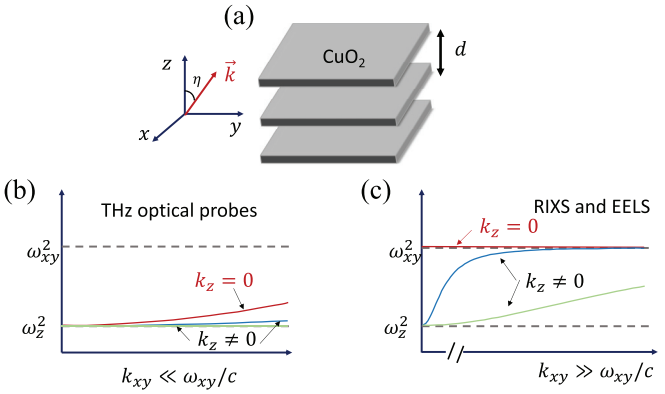

FIG. 1. (a) Basic notation used in the paper to describe a layered superconductor. SC sheets are parallel to the xy plane and stacked along z, at distance d. Within the context of cuprates, the SC planes correspond to the crystallographic CuO_2 planes. The angle that the wave vector forms with the z axis will be denoted with η. (b), (c) Plasmon dispersion for a layered superconductor discussed so far in the literature. Panel (b) shows the dispersion Eq. (1) that is expected to describe the plasma dispersion near the low-energy out-of-plane plasmon ω_z and for momenta much smaller than the scale set by the light cone for the largest plasma frequency. It has been derived [14,15,25–28] within several papers focusing on the dynamics of the out-of-plane SC phase, in relation to the THz optical response of the Josephson plasmon. Panel (c) shows instead the dispersion Eq. (2) that is expected to describe the plasma dispersion near the high-energy in-plane plasmon ω_{xy}. It is has been derived by studying the generic in-plane and out-of-plane phase or density dynamics in the SC phase [10,11,13,20,30], and it corresponds to the standard result for the layered electron gas [31–34], used to interpret RIXS or EELS experiments, which probes relatively high momenta and energy.

magnitude in some families of cuprates, and k_{xy}, k_z denote the in-plane and out-of-plane momenta, respectively. Equation (1) is sketched in Fig. 1(b) as a function of k_{xy} at various values of k_z. As evident from Eq. (1), it represents a regular function of $\mathbf{k}$ which tends always to ω_z as $\mathbf{k} \to 0$. As we will discuss in detail below, even though this mode corresponds to light polarized mainly along z, at an arbitrary wave vector it has a mixed transverse and longitudinal character, while a purely longitudinal and transverse character is only recovered when $k_{xy} = 0$ or $k_z = 0$, respectively. The undamped nature of this propagating mode in the SC state recently motivated several proposals of possible applications. From one side, the inherent nonlinearity of the Josephson coupling among CuO_2 planes may enable nonlinear photonic applications based on the the use of intense THz laser pulses, as widely addressed both experimentally [15,35–38] and theoretically [14,28,39–41]. From the other side, low-energy Josephson plasmons can be attractive for photonic applications based on near-field nano-optics [4,5,42,43] that also focus on the regime of few THz and small $k \ll \omega_{xy}/c$ momenta.

While optics is interested in the limit of long wavelength, other spectroscopic probes like resonant x-ray scattering (RIXS) and electron energy-loss spectroscopy (EELS) are mostly able to detect the plasma dispersion around ω_{xy} and relatively larger momenta $k \gg \omega_{xy}/c$ as compared to the scale set by the light cone [44]. In this regime, the effects of anisotropy have been mainly discussed focusing on the emergence of acousticlike branches of plasma excitations dispersing below ω_{xy}, see Fig. 1(c). In this case, theoretical calculations focusing on the SC state derived the plasma dispersion either looking at the dynamics of the (in-plane and out-of-plane) SC phase [10–13] or at the dynamics of the density [20,30]. In both cases, the standard result is fully analogous to the one found for the metallic state by means of the layered electronic model in the presence of Coulomb interactions [31–34], and reduces to a plasma dispersion given by

$$\omega_p^2(\mathbf{k}) = \omega_{xy}^2 \frac{k_{xy}^2}{k^2} + \omega_z^2 \frac{k_z^2}{k^2}, \tag{2}$$

where an additional $\sim v_P^2 k^2$ term, relevant to describe the plasmon dispersion with velocity v_P at $k_z = 0$, can be added [13]. As one can see in Fig. 1(c), at finite k_z there is an intermediate regime of k_{xy} values where the plasmon softens below ω_{xy}, crossing from a quasilinear to a $\omega \propto \sqrt{k}$ behavior, typical of two-dimensional plasmons. So far, such acousticlike branches have been identified by RIXS in some high-temperature cuprates [45–47], while EELS observed only the high-energy optical branch, with a strong and still not well-understood overdamping [48–51]. Despite the fairly good agreement between Eq. (2) and RIXS experiments, which probe energies around ω_{xy} and large momenta as compared to ω_{xy}/c, there is apparently no connection between Eq. (2) and the expression Eq. (1), which should represent the limit of the plasma dispersion when one focuses around ω_z and small momenta. Indeed, in contrast to Eq. (1), Eq. (2) is nonanalytic as $\mathbf{k} \to 0$, since it predicts a continuum of possible values which depend on the angle that the wave vector $\mathbf{k}$ forms with the z axis. In addition, at $k_z = 0$ and finite k_{xy}, as shown in Figs. 1(b) and 1(c), Eq. (1) predicts a mode dispersing away from the soft Josephson plasmon ω_z while Eq. (2) (with the additional $v_P^2 k^2$ term) predicts a mode around ω_{xy}.

In this paper, we provide a general derivation of the plasma dispersion in a layered superconductor which is valid at generic momentum, and we identify a crossover value $k_c = \sqrt{(\omega_{xy}^2 - \omega_z^2)}/c$ such that the two previously reported expressions Eqs. (1) and (2) emerge as the limit of small $k \ll k_c$ or large $k \gg k_c$ momentum of the full dispersion. To this aim, we analyze the problem focusing on the degrees of freedom linked to the SC phase of the order parameter within an effective-action formalism, which naturally implements the spontaneous symmetry breaking below T_c. We introduce explicitly the electromagnetic (e.m.) scalar and vector potentials to construct a gauge-invariant (g.i.) quantum action for the coupled system given by the matter (represented by the SC phase) and the e.m. fields. The main technical difference with respect to previous work using the same formalism [10,11,13], that was able to only obtain the result Eq. (2), relies on the fact that for an anisotropic superconductor, the role of e.m. interactions is not exhausted by the Coulomb interaction, which originates from the scalar potential. The reason is that, as one already observes at the level of Maxwell equations [25–27,29,39], in a layered system the e.m. longitudinal and transverse response get intrinsically mixed, unless light propagates along the main crystallographic axes.

The physical reason is that once the superfluid response is anisotropic, the induced current is no more parallel to the electric field. Within the context of the SC phase dynamics, the anisotropy of the superfluid response leads, in contrast to the isotropic case, to a finite coupling of phase fluctuations to both the longitudinal and transverse components of the e.m. fields. When both couplings are properly included, the phase spectrum at an arbitrary wave vector carries on the information on a mixed longitudinal-transverse excitation, except for the two special limits ($k_{xy} \to 0, k_z = 0$) or ($k_{xy} = 0, k_z \to 0$). By introducing an appropriate g.i. phase variables, we can derive an analytical expression for the generalized plasma modes valid at generic momentum. In particular, the mode lower in energy, that becomes purely longitudinal only well above k_c, is shown to interpolate among the two limiting behaviors provided by Eqs. (1) and (2), then clarifying the limits of their validity. In addition, such a formulation allows one to easily extend the result to the case of a nonlinear Josephson model, as previously discussed within the context of the out-of-plane Josephson plasmon [25–27,29,39]. Finally, to make a closer connection with experimental probes sensitive to density correlations [44], we explicitly derive the density-density response in the general case, showing that both generalized plasma modes appear in the spectrum of the physical observables, with an equal weight at the length scale $\sim 1/k_c$, which is typically of the order of a fraction of micron. At larger momenta $k \gg k_c$, the density response closely matches the standard random-phase approximation (RPA) result, as derived both for layered metals [31–34] and layered superconductors [10,11,13,20,30], and a single quasilongitudinal plasma mode visible in the density spectral function. Since the crossover scale k_c vanishes for the light velocity c going to infinity, the failure of the standard RPA result at an arbitrary wave-vector propagation stems from the relevance of relativistic effects at low momenta. Our results represent a complete g.i. description of generalized plasma excitations in a layered superconductor valid at different energy and momentum scales, providing a benchmark behavior to analyze plasmonic effects in a wide set of experiments ranging from near-field optics to RIXS and EELS.

The paper is as follows: In Sec. II, we review the standard derivation of the Gaussian phase-only action in the isotropic case. The section starts with an introductory subsection where we outline the theoretical approach used in the paper, and a second one where we show its application in the standard isotropic case. Here we show that the plasma mode appears in the different sectors of the matter-e.m. field action depending on the gauge choice, but always leading to the same result. The results of this section are not new, but their derivation is carried out in a different way with respect to previous work, and it allows us to introduce the formalism relevant for the rest of the paper. In Sec. III, we derive the action for the layered 3D case, expressed in terms of the appropriate g.i. variables. We then show that the longitudinal and transverse e.m. excitations are always coupled, and both excitations appear in the phase spectrum at an arbitrary wave-vector propagation, with the exception of the two cases of light propagating purely in plane or out-of-plane. A simplified description of the problem within the context of the Maxwell's equation is also provided in Appendix B. In Sec. III C, we rephrase the same results in terms of approximate equations of motion, that have been widely used in the recent literature [14,15,25–29] to include nonlinear effects of the plasmon dynamics. In Sec. IV, we show how the mixed longitudinal-transverse modes found in Sec. III also appear as poles of the properly computed density-density response function. Section V contains a general discussion about the results. Further technical details are provided in the Appendices. Appendix A reviews the main steps leading to the effective action for a superconductor within the functional-integral formalism. Appendix B shows the derivation of the mixed longitudinal-transverse modes from the solution of the Maxwell's equations.

II. EFFECTIVE ACTION FOR THE ISOTROPIC CASE

A. Description of the plasmon via the SC phase

Before giving technical details about the derivation of the plasma dispersion for the layered superconductor, it can be useful to briefly outline the general context, starting from the isotropic case. As mentioned in the Introduction, the SC transition carries specific signatures both in the single-particle fermionic excitations spectrum, via the opening of the SC gap below T_c, and in the spectrum of the bosoniclike collective excitations. More specifically, while the gap is connected to the equilibrium value of the SC complex order parameter, two modes emerge connected to fluctuations of its amplitude and phase. Since the SC order parameter breaks the continuous gauge symmetry, a Goldstone mode is expected that is directly linked to phase fluctuations of the SC order parameter [6]. There are several ways to see this. At the level of the classical Ginzburg-Landau description, this appears as an energetic cost needed to twist the phase θ with respect to its equilibrium value. In full analogy with the elastic deformation of a solid body, the cost E of a finite phase gradient *in space* scales with a superfluidstiffness D_s, such that

$$E = \frac{\hbar^2 D_s}{8} \int d\mathbf{x} (\nabla\theta)^2. \tag{3}$$

In the simplest Galilean-invariant case, D_s can be expressed as the ratio between the density of superfluid electrons and their mass, $D_s = n_s/m$, with $n_s = n$ at $T = 0$. As the length scale of spatial phase deformations goes to infinity, E vanishes. This can be interpreted as a mode at zero energy for $\mathbf{k} = 0$, as expected for a Goldstone mode. On the other hand, to really define a propagating mode, i.e., to establish a frequency-momentum dispersion, one needs to include dynamical effects, not present in the classical Ginzburg-Landau description. A very elegant and powerful technique relies [6] on the explicit construction of a quantum analogous of the Ginzburg-Landau model by starting from a microscopic interacting model for electrons. The basic idea is to start from a fermionic model with a BCS-like interaction term and decouple it via the Hubbard-Stratonovich (HS) procedure by introducing two effective bosonic fields which play the role of the order-parameter amplitude and phase. By further explicitly integrating out the fermions, one obtains a quantum model expressed in terms of the collective SC variables that can be expanded in principle up to arbitrary powers in the collective-mode fields, linking the phenomenological couplings of the Ginzburg-Landau model to fermionic susceptibilities, which

contain all the information on the microscopic physics under investigation. Such a procedure is outlined in Appendix A, and further details can be found in several books and papers on the subject, see, e.g., Ref.s [6,8–13]. By retaining only Gaussian terms in the fluctuations, one defines the spectrum of the collective modes, equivalent to compute the response functions at the RPA level in the usual diagrammatic approach to fermionic models [2,6]. Within this quantum generalization of the classical Ginzburg-Landau theory, one finds that the density appears as a conjugate variable of the phase [6,8,9]. As a consequence, within the quantum phase-only action, the energetic cost to perform a phase gradient *in time* is controlled by the charge compressibility κ_0 [8,9], and Eq. (3) is replaced at $T = 0$ by the quantum action:

$$S = \frac{\hbar^2}{8} \int dt d\mathbf{x} [\kappa_0 (\partial_t \theta)^2 - D_s (\nabla \theta)^2]. \tag{4}$$

For weakly interacting neutral systems, κ_0 in the static long-wavelength limit can be approximated with the density of states at the Fermi level, and in Eq. (4) one recognizes the so-called [7] Anderson-Bogoliubov sound mode,

$$\omega^2 = v_s^2 |\mathbf{k}|^2, \tag{5}$$

where $v_s^2 = D_s/\kappa_0$ is the sound velocity.

The identification of the density as a conjugate variable of the phase is a general result, which holds both for neutral superfluids and for superconductors, and has profound implications for the latter. Indeed, in the standard description of charged systems, density-density interactions are expected to be mediated by the long-range Coulomb potential. In literature based on the effective-action formalism, the difference between neutral and charged superfluids is then usually encoded [6,9–13] via an additional HS field which decouples density-density fermionic interactions, so its integration dresses the charge compressibility at RPA level by the Coulomb potential [7]. The term κ_0 in Eq. (4) is then replaced in Fourier space by $\kappa(\mathbf{k}) = \kappa_0/(1 + V(\mathbf{k})\kappa_0)$, where $V(\mathbf{k})$ is the Coulomb potential in generic D dimensions. Since for $\mathbf{k} \to 0$ one has $\kappa \to 1/V(\mathbf{k})$, the spectrum of the phase mode that reflects one of the density fluctuations now identifies a plasma mode, whose energy versus momentum dispersion depends on the dimensions. In the standard isotropic three-dimensional (3D) case, one recovers the well-known dispersion

$$\omega^2 = \omega_p^2 + v_s^2 |\mathbf{k}|^2, \tag{6}$$

where $\omega_p^2 = 4\pi e^2 D_s$ is the isotropic plasma frequency.

The procedure outlined above explains why in the SC state the spectrum of the collective plasma excitations can be derived in a relatively simple way by analyzing the SC phase fluctuations. However, this analysis is not enough if one wants to determine the spectral weight of the plasma mode, that can only be determined by direct derivation of the density-density response [6,10,12,13], which couples to external probes. Indeed, on a more general ground, the SC phase itself does not represent a physically observable quantity. Once the matter is coupled to the e.m. field, the physical observables are related to the g.i. four-vector ψ_μ, whose temporal and spatial components read

$$\psi_0 \equiv \partial_t \theta + \frac{2e}{\hbar}\phi \quad \boldsymbol{\psi} \equiv \nabla\theta - \frac{2e}{\hbar c}\mathbf{A}, \tag{7}$$

where ϕ and $\mathbf{A}$ are the scalar and vector potentials, respectively. In contrast to the phase alone, the observables Eq. (7) are invariant under the simultaneous gauge transformation of the e.m. potentials (that leaves the physical electrical and magnetic field unchanged) and of the SC phase:

$$\begin{aligned} \theta(\mathbf{x}, t) &\to \theta(\mathbf{x}, t) + \frac{2e}{\hbar c}\lambda(\mathbf{x}, t) \\ \mathbf{A}(\mathbf{x}, t) &\to \mathbf{A}(\mathbf{x}, t) + \nabla\lambda(\mathbf{x}, t) \\ \phi(\mathbf{x}, t) &\to \phi(\mathbf{x}, t) - \partial_t \lambda(\mathbf{x}, t). \end{aligned} \tag{8}$$

In this picture, one realizes that analyzing the spectrum of the phase mode in the superconductor is completely equivalent to solving the problem of the e.m. wave propagation. More specifically, the frequency-momentum relation Eq. (6) corresponds to the one of the longitudinal component of the electric field, which couples by Maxwell's equations to charge fluctuations and then to phase fluctuations in a superconductor. In general, e.m. waves can also be transverse, but in the isotropic system they are not coupled to phase fluctuations. Once again, this result can be easily understood already at classical level. In isotropic and homogeneous systems, the minimal-coupling substitution Eq. (7) into the gradient term Eq. (3) leads to

$$E = \frac{\hbar^2 D_s}{8} \int d\mathbf{x} \left(\nabla\theta - \frac{2e}{\hbar c}\mathbf{A} \right)^2. \tag{9}$$

The explicit coupling among the phase and the gauge field in Eq. (4) is the term $\int d\mathbf{x} D_s (\nabla\theta) \cdot \mathbf{A}$, that for a constant D_s can be written after integrating by part as $\int d\mathbf{x}\, D_s \theta (\nabla \cdot \mathbf{A})$. As a consequence, the phase couples *only* to the longitudinal component of the e.m. field, and one does not see any signature of the transverse e.m. mode in the phase spectrum. Such a decoupling of the longitudinal and transverse sectors makes the description of the plasma mode completely equivalent in the two approaches: via the matter, where the charged nature of the system enters via the Coulomb interaction for the density, or via e.m. potentials, where one derives directly the equations of motions for the e.m. fields.

The situation becomes radically different for *anisotropic* systems and, in particular, for layered superconductors. In this case, which is relevant for several classes of unconventional superconductors, as, e.g., cuprates or pnictides, the phase stiffness in plane $D_\parallel$ and in the direction perpendicular to planes $D_\perp$ is anisotropic, with $D_\perp \ll D_\parallel$ [17–19]. Within the language of Eq. (9) above, this implies that the phase can also be coupled to the transverse vector potential. This is the central physical effect which motivates the present paper, aimed at explaining what the consequences are of such a mixing of the transverse and longitudinal modes for the spectrum of plasma waves. Indeed, as we mentioned in the Introduction, so far the effect of this mixing has been included in an approximated way in the work [25–27] aimed to derive the dispersion Eq. (1) of the soft Josephson plasmon, but it is completely missing in any approach extending the RPA to the layered electron gas [31–34] or to the layered superconductors [10,11,13,20,30]. Indeed, the standard RPA approximation is

usually implemented by computing the charge response only to the scalar Coulomb potential, then writing the full density response as a resummation of bubblelike diagrams representing the bare density response, and leading to the expression Eq. (2) for the layered plasmon. Since the Coulomb potential is linked to the longitudinal component of the e.m. field, this is equivalent to neglect any correction to the charge response induced by the transverse vector potential, that is, however, an approximation in the case of a layered system for arbitrary wave-vector propagation.

In Sec. III, we will explicitly show how the transverse-longitudinal mixing appears in the quantum phase-only model for the layered superconductor, and how one can derive from it an analytical expression for the generalized plasma dispersion which interpolates between the two limits Eqs. (1) and (2), clarifying at the same time their range of validity. To get better insight into the link among the phase mode and the plasma wave, we will first review in the next subsection the isotropic case. In contrast to previous work [6,9–11,13] where the e.m. field only enters via the Coulomb density-density interaction, we introduce here the coupling Eq. (7) of the SC phase to the internal e.m. field that we further integrate out. We then show how the same plasmon dispersion is obtained regardless of the gauge choice for the e.m. field, as expected. This approach will then be extended to the layered case in Sec. III.

B. Formulation of the problem with the internal e.m. fields

As a starting point, we use the imaginary-time equivalent of the quantum action Eq. (4) for an isotropic 3D superconductor, rewritten in Fourier space. As mentioned above, its derivation relies on a rather standard technique [6,8–13], whose details are given in Appendix A. We then have

$$S_G[\theta] = \frac{1}{8}\sum_q \left[\kappa_0 \Omega_m^2 + D_s|\mathbf{k}|^2\right]|\theta(q)|^2, \tag{10}$$

where $q \equiv (i\Omega_m, \mathbf{k})$ is the imaginary-time four-momentum, $\Omega_m = 2\pi m T$ are bosonic Matsubara frequencies, κ_0 is the bare compressibility, and D_s is the superfluid stiffness. In the following, we put $\hbar = k_B = 1$. In ordinary Maxwell equations, the source for the e.m. fields is provided both by external charge and currents and by the induced internal charge and current fluctuations in the matter. In the superconductor, the latter will be described by the SC phase, coupled to the internal e.m. fields via the minimal coupling Eq. (7). To account for the e.m. fields, we then need to first include the free contribution, which reads [6]

$$\begin{aligned} S_{\text{e.m.}}[A_\mu] &= \int d\tau d\mathbf{x}\left[\frac{(\nabla\times\mathbf{A})^2}{8\pi} - \frac{\varepsilon}{8\pi}\left(\frac{i\partial_\tau \mathbf{A}}{c} + \nabla\phi\right)^2\right] \\ &= \frac{\varepsilon}{8\pi}\sum_q \left[\frac{\Omega_m^2}{c^2}|\mathbf{A}(q)|^2 - |\mathbf{k}|^2|\phi(q)|^2\right. \\ &\quad + \frac{|\mathbf{k}|^2}{\varepsilon}|\mathbf{A}_T(q)|^2 \\ &\quad \left. + \frac{i\Omega_m}{c}\mathbf{k}\cdot(\phi(q)\mathbf{A}_L(-q) + \phi(-q)\mathbf{A}_L(q))\right]. \end{aligned} \tag{11}$$

Here we introduced the longitudinal $\mathbf{A}_L = (\hat{\mathbf{k}}\cdot\mathbf{A})\hat{\mathbf{k}}$ and transverse $\mathbf{A}_T = \mathbf{A} - \mathbf{A}_L = (\hat{\mathbf{k}}\times\mathbf{A})\times\hat{\mathbf{k}}$ components of $\mathbf{A}$. Equation (11) is just a transcription of the usual form $\frac{-|\varepsilon\mathbf{E}|^2+|\mathbf{B}|^2}{8\pi}$, where the electric field is expressed in the imaginary-time formalism as $\mathbf{E} = -\frac{i}{c}\partial_\tau\mathbf{A} - \nabla\phi$. It is worth noting that to have a definition of $\mathbf{E}$ analogous to the one valid for real time, one should assume that ϕ is purely imaginary, i.e., one should replace $\phi \to i\phi$. In this case, by defining the imaginary-time electric field as $\mathbf{E} \equiv -\frac{1}{c}\partial_\tau\mathbf{A} - \nabla\phi$, the action for the free e.m. field would read $\frac{\varepsilon|\mathbf{E}|^2+|\mathbf{B}|^2}{8\pi}$, which is the usual expression for the energy density. Such a rescaling of the scalar potential would also make the quadratic term in the scalar potential arising from $(\nabla\phi)^2$ positive defined, as required to perform the Gaussian integration. To make the notation more compact, we will not explicitly rescale the potential in what follows, but we will implicitly assume that a formal definition of the Gaussian integration in the imaginary-time formalism requires such a regularization. To include the ionic screening, we also introduced the background dielectric constant ε. As mentioned above, in the superconductor [6,9,10,12] the coupling of the e.m. radiation with the matter can be easily implemented by using the SC phase, via the minimal coupling substitution Eq. (7), which reads in momentum space and Matsubara frequency:

$$\begin{aligned} \Omega_m\theta(q) &\to \Omega_m\theta(q) + 2e\phi(q) \\ i\mathbf{k}\theta(q) &\to i\mathbf{k}\theta(q) - \frac{2e}{c}\mathbf{A}(q). \end{aligned} \tag{12}$$

By replacing Eqs. (12) into the action Eq. (10), one obtains a light-matter coupling term $S_{\theta A_\mu}[\theta, A_\mu]$ and a renormalization of the bare e.m. action, so the total action reads

$$S[\theta, A_\mu] = S_G[\theta] + S'_{\text{e.m.}}[A_\mu] + S_{\theta A_\mu}[\theta, A_\mu], \tag{13}$$

where $S'_{\text{e.m.}}[A_\mu]$ describes the long-wavelength propagation of light through matter. For the isotropic system, this term reads

$$\begin{aligned} S'_{\text{e.m.}}[A_\mu] = \frac{\varepsilon}{8\pi}\sum_q \Bigg[&-\left(|\mathbf{k}|^2 + k_{\text{TF}}^2\right)|\phi(q)|^2 \\ &+ \left(\Omega_m^2 + \omega_p^2\right)\frac{|\mathbf{A}_L(q)|^2}{c^2} \\ &+ \left(\Omega_m + \frac{c^2}{\varepsilon}|\mathbf{k}|^2 + \omega_p^2\right)\frac{|\mathbf{A}_T(q)|^2}{c^2} \\ &+ \frac{2i\Omega_m}{c}\mathbf{k}\cdot(\phi(q)\mathbf{A}_L(-q) + \phi(-q)\mathbf{A}_L(q))\Bigg]. \end{aligned} \tag{14}$$

In the effective-action formalism, the frequency-momentum dispersion obtained as a solution of the Maxwell's equations appears as the zero of the determinant of the matrix associated with the coefficients of the fields in the Gaussian action, once the analytical continuation $i\Omega_n \to \omega + i\delta$ is performed. As a consequence, one clearly sees that the inclusion of the matter has two well-known effects on the e.m. fields: (i) the scalar potential displays the usual Thomas-Fermi screening, where $k_{\text{TF}}^2 = 4\pi e^2\kappa_0/\varepsilon$; (ii) the propagating transverse mode

$$\omega_T^2 = \omega_p^2 + \tilde{c}^2|\mathbf{k}|^2 \tag{15}$$

is gapped out [52] at the isotropic (screened) SC plasma frequency

$$\omega_p^2 \equiv 4\pi e^2 D_s/\varepsilon, \tag{16}$$

and the light velocity is renormalized as $\tilde{c} = c/\sqrt{\varepsilon}$. In the typical field-theory language, the Anderson-Higgs mechanism [52] manifest as a mass term $\omega_p^2 \mathbf{A}_T^2$ in the e.m. action Eq. (14), that, in the static limit, only survives below T_c, where $D_s \neq 0$. Finally, the coupling between the phase and the e.m. potential reads

$$S_{\theta A_\mu}[\theta, A_\mu] = \frac{e}{4}\sum_q \Big[\kappa_0 \Omega_m(\theta(q)\phi(-q) - \theta(-q)\phi(q)) - i\frac{D_s}{c}\mathbf{k}\cdot(\theta(q)\mathbf{A}_L(-q) - \theta(-q)\mathbf{A}_L(q))\Big]. \tag{17}$$

The last term of Eq. (17) shows explicitly that in the isotropic case phase fluctuations only couple to the longitudinal component of the vector potential $\mathbf{A}_L$, as mentioned above. In addition, the use of Eq. (12) clearly guarantees that the total action is invariant under the gauge transformation Eq, (8), which reads explicitly in Matsubara formalism:

$$\begin{aligned}\theta(q) &\to \theta(q) + \frac{2e}{c}\lambda(q)\\ \phi(q) &\to \phi(q) - \frac{\Omega_m}{c}\lambda(q)\\ \mathbf{A}(q) &\to \mathbf{A}(q) + i\mathbf{k}\lambda(q);\end{aligned} \tag{18}$$

$\lambda(q)$ being an arbitrary function of the Fourier momenta. Such a gauge freedom also implies that only the g.i. combination Eq. (12) represents a physically observable quantity describing matter properties, while the information carried out by the SC phase alone acquires a different meaning within different gauge choices. This means that even though the phase-only propagator is always linked to the plasma mode, it will appear in different forms, depending on the gauge.

To clarify this point, let us start from Eq. (13) and derive the action for the phase degrees of freedom by integrating out the e.m. potentials. A first natural gauge choice is the so-called Coulomb gauge $\nabla\cdot\mathbf{A} = 0$, i.e., $\mathbf{A}_L = 0$. Indeed, as noted below Eq. (17), in the isotropic case the phase fluctuations only couple to $\mathbf{A}_L$ so, in the Coulomb gauge, only the coupling between the phase and the scalar potential survives. By integrating out ϕ, one is then left with

$$S^{(\mathrm{iso})}_{\nabla\cdot\mathbf{A}=0} = \frac{\varepsilon}{32\pi e^2}\sum_q \left[\frac{\Omega_m^2}{1+\alpha|\mathbf{k}|^2} + \omega_p^2\right]|\mathbf{k}|^2|\theta(q)|^2, \tag{19}$$

where we defined α as

$$\alpha \equiv \frac{\varepsilon}{(4\pi e^2\kappa_0)} = \frac{1}{k_{\mathrm{TF}}^2} = \lambda_D^2, \tag{20}$$

where λ_D is the Debye screening length. The result Eq. (19) is formally identical to the one widely discussed in previous literature [6,9,10,12,13], and obtained by adding a Coulomb-mediated density-density interaction term in the starting microscopic fermionic model. This is a natural consequence of the fact that in the Coulomb gauge only the coupling of the phase to the scalar potential is relevant.

An alternative but completely equivalent approach can be followed integrating out the e.m. fields in the Weyl gauge, where $\phi = 0$. In this case, only the coupling to $\mathbf{A}_L$ survives in Eq. (17) and one obtains

$$S^{(iso)}_{\phi=0} = \frac{\kappa_0}{8}\sum_q \frac{\Omega_m^2}{\Omega_m^2+\omega_p^2}\left[\Omega_m^2 + (1+\alpha|\mathbf{k}|^2)\omega_p^2\right]|\theta(q)|^2. \tag{21}$$

We immediately see that both Eqs. (19) and (21) identify a collective excitation as a pole of the $\theta(q)$ fluctuations, which are controlled by the inverse of the $|\theta(q)|^2$ term. After analytical continuations to real frequencies, this is given by

$$\omega^2 = \omega_p^2(1+\alpha|\mathbf{k}|^2), \tag{22}$$

that is, the usual dispersion of the longitudinal plasma mode in a superconductor. As usual, the plasmon velocity $c_p = \sqrt{\alpha}\omega_p = \tilde{c}(\lambda_D/\lambda)$, where λ is the London penetration depth, is much smaller than the light velocity $\tilde{c}$ of the transverse wave in the medium, since $\lambda_D/\lambda \ll 1$ even for unconventional superconductors. It is worth noting that the velocity of the plasmon in Eq. (22) is not the same as the one obtained for the normal metal [3] that would correspond to $\omega^2 = \omega_p^2(1+(9/5)\alpha|\mathbf{k}|^2)$. This is due to the fact that to correctly account for the plasma dispersion, one should also account for the $|\mathbf{k}|^2$ corrections to the BCS density-density response function in the SC state that appears as a coefficient of the $(\partial_t\theta)^2$ term in the phase-only action, while in Eq. (4) only its long wave-length limit κ_0 has been retained. To simplify the notation, we shall not explicitly perform such an expansion that is anyway irrelevant to the physical effects we want to discuss in the present paper. Indeed, it only gives a small quantitative difference that can be included if one is interested in a detailed quantitative comparison with the experiments.

While in Eq. (19) the plasma mode appears in the spectrum of $\nabla\theta$ fluctuations, in the Weyl gauge it appears in the spectrum of $\partial_\tau\theta$ fluctuations. This is a direct consequence of the fact that the phase variable does not represent a true physical observable. In addition, it describes, as expected, only the longitudinal mode. For both gauge choices, the transverse e.m. mode is described by the two remaining degrees of freedom of the e.m. field in Eq. (13). A very elegant and convenient way to simultaneously derive the energy-momentum dispersion for all the transverse and longitudinal e.m. modes relies on the use of the g.i. physical observables Eq. (7). For example, one can use the spatial component of the g.i. phase difference,

$$\boldsymbol{\psi} = \nabla\theta - \frac{2e}{c}\mathbf{A}, \tag{23}$$

and set to zero the scalar component via a proper gauge fixing. The equivalent of Eq. (13) in the new variables reads

$$S[\theta,\boldsymbol{\psi}] = \frac{\varepsilon}{32\pi e^2}\sum_q \Big[\big(\Omega_m^2+\omega_p^2\big)|\boldsymbol{\psi}(q)|^2 + \tilde{c}^2|\mathbf{k}\times\boldsymbol{\psi}|^2 + \frac{\Omega_m^2}{\alpha}(1+\alpha|\mathbf{k}|^2)|\theta(q)|^2 + i\Omega_m^2\mathbf{k}\cdot(\boldsymbol{\psi}(q)\theta(-q) - \boldsymbol{\psi}(-q)\theta(q))\Big]. \tag{24}$$

By introducing again the longitudinal $\boldsymbol{\psi}_L = (\hat{\mathbf{k}}\cdot\boldsymbol{\psi})\hat{\mathbf{k}}$ and the transverse $\boldsymbol{\psi}_T = \boldsymbol{\psi} - \boldsymbol{\psi}_L = (\hat{\mathbf{k}}\times\boldsymbol{\psi})\times\hat{\mathbf{k}}$ components, we see that only $\boldsymbol{\psi}_L$ couples to the phase θ. After integrating it out, one then finds

$$S[\boldsymbol{\psi}] = \frac{\varepsilon}{32\pi e^2}\sum_q \left[\left(\frac{\Omega_m^2}{1+\alpha|\mathbf{k}|^2}+\omega_p^2\right)|\boldsymbol{\psi}_L(q)|^2 + \left(\Omega_m^2+\omega_p^2+\tilde{c}^2|\mathbf{k}|^2\right)|\boldsymbol{\psi}_T(q)|^2\right]. \tag{25}$$

From Eq. (25), one immediately sees that the three components of $\boldsymbol{\psi}$ describes all e.m. modes, as given by the poles of the longitudinal and transverse propagators. Indeed, after analytical continuation, one finds the solution Eq. (22) in the longitudinal sector and the solution Eq. (15) in the transverse sector, respectively. Such a result suggests that in the anisotropic case where longitudinal and transverse modes get mixed, a description in terms of the physical fields Eq. (23) can be more convenient, as we shall indeed see in the next section. In addition, this choice will make the extension of the Gaussian action to a nonlinear Josephson model straightforward, since it will only affect the mass term for the $\boldsymbol{\psi}$ field, as we will see in detail in Sec. III C.

III. EFFECTIVE ACTION FOR A LAYERED 3D SYSTEM

A. Derivation of the plasma dispersion for the anisotropic system

To discuss the layered case, we should consider an extension of Eq. (10) where the stiffness is anisotropic. By using the notation of Fig. 1(a), we will denote with D_{xy} and D_z the in-plane and out-of-plane stiffness, respectively. Equation (10) can be straightforwardly generalized [10,11,13] to

$$S_G[\theta] = \frac{1}{8}\sum_q \left[\kappa_0\Omega_m^2 + D_{xy}k_{xy}^2 + D_z k_z^2\right]\theta(q)\theta(-q), \tag{26}$$

where $k_{xy}\equiv\sqrt{k_x^2+k_y^2}$ is the in-plane momentum. Note that, despite the discrete out-of-plane structure of the system, we still use a continuum anisotropic model, as valid when $k_z \ll 1/d$. Indeed, the breakdown of the standard RPA approximation and the mixing between longitudinal and transverse degrees of freedom, which will be the main topics of this section, occur at very small momenta $\mathbf{k}$, which are suitably accounted for in the continuum limit. The anisotropy of the stiffness has important consequences when the electrons are coupled to the e.m. fields via the minimal-coupling substitution Eq. (12). Indeed, the action Eq. (14) describing the e.m. field in the matter gets modified as

$$S'_{\text{e.m.}}[A_\mu] = \frac{\varepsilon}{8\pi}\sum_q \left[-\left(k_{\text{TF}}^2+|\mathbf{k}|^2\right)|\phi(q)|^2 + \frac{1}{\varepsilon}|\mathbf{k}\times\mathbf{A}(q)|^2 + \frac{\left(\Omega_m^2+\omega_{xy}^2\right)}{c^2}|\mathbf{A}_{xy}(q)|^2 + \frac{\left(\Omega_m^2+\omega_z^2\right)}{c^2}|\mathbf{A}_z(q)|^2 + \frac{2i\Omega_m}{c}\phi(q)\mathbf{k}\cdot\mathbf{A}(-q) - \text{H.c.}\right], \tag{27}$$

where we defined the two plasma frequencies:

$$\omega_{xy}^2 = \frac{4\pi e^2 D_{xy}}{\varepsilon}, \quad \omega_z^2 = \frac{4\pi e^2 D_z}{\varepsilon}. \tag{28}$$

In principle, in Eq. (27) we could also consider an anisotropic background dielectric constant to take into account the different ionic screening occurring along the in-plane and out-of-plane directions. The e.m. energy density would then read $\frac{-\varepsilon_\alpha|\mathbf{E}_\alpha|^2+|\mathbf{B}|^2}{8\pi}$, with $\varepsilon_\alpha = \varepsilon_{xy}$ for $\alpha = x, y$, and $\varepsilon_\alpha = \varepsilon_z$ for $\alpha = z$. However, this effect does not substantially modify the physics of the system; therefore, for the sake of simplicity we take ε to be isotropic.

Finally, the coupling of the e.m. fields with the phase variable is an anisotropic version of Eq. (17), that is now expressed as

$$S_{\theta A_\mu}[\theta, A_\mu] = \frac{e}{4}\sum_q \left[\kappa_0\Omega_m\theta(q)\phi(-q) + \text{H.c.} - \frac{D_{xy}}{c}i\theta(q)\mathbf{k}_{xy}\cdot\mathbf{A}_{xy}(-q) + \text{H.c.} - \frac{D_z}{c}i\theta(q)\mathbf{k}_z\cdot\mathbf{A}_z(-q) + \text{H.c.}\right]. \tag{29}$$

As one can see, the anisotropy of the SC phase stiffness has two main consequences in the description of the e.m. response: (i) the massive terms in the vector potential of Eq. (27) become anisotropic and (ii) the inclusion of the matter via the SC phase shows that there is no way to decouple completely the longitudinal and transverse modes at arbitrary wave vector $\mathbf{k}$. The latter result emerges more clearly by close inspection of Eq. (29). While in the isotropic case, the equivalent term $D_s\mathbf{k}\cdot\mathbf{A}$ of Eq. (17) implies that θ only couples to the longitudinal component of the vector potential, in the anisotropic case the combination $D_{xy}\mathbf{k}_{xy}\cdot\mathbf{A}_{xy} + D_z\mathbf{k}_z\cdot\mathbf{A}_z$ is different from zero even in the Coulomb gauge where $\mathbf{k}\cdot\mathbf{A} = 0$, unless of course propagation occurs purely in plane ($k_z = 0$) or out of plane ($k_{xy} = 0$). This is the crucial point that has been missed in previous work where the effect of the anisotropy has been only included in the phase stiffness but not on the coupling to the gauge potential. At a more general level, the physical effect we are implementing here is the fact that the superfluid current is no more parallel to to electric field, so even a purely longitudinal field always induces a transverse current and vice versa. Such an interpretation is straightforward when the problem is studied via Maxwell's equations only, as we discuss in Appendix B.

To better understand the consequences of the coupling between transverse and longitudinal modes, let us first recall the derivation of the standard result Eq. (2). If one uses the Coulomb gauge and retains in Eq. (29) only the coupling to the scalar potential ϕ, the effect of its integration is a straightforward generalization of Eq. (19), provided that one accounts for the anisotropy of the stiffness of Eq. (26). The action for the phase would then read

$$S^{(\text{ani})}_{\nabla\cdot\mathbf{A}=0} \simeq \frac{\varepsilon}{32\pi e^2}\sum_q \left[\frac{\Omega_m^2|\mathbf{k}|^2}{1+\alpha|\mathbf{k}|^2} + \omega_{xy}^2k_{xy}^2 + \omega_z^2k_z^2\right]|\theta(q)|^2. \tag{30}$$

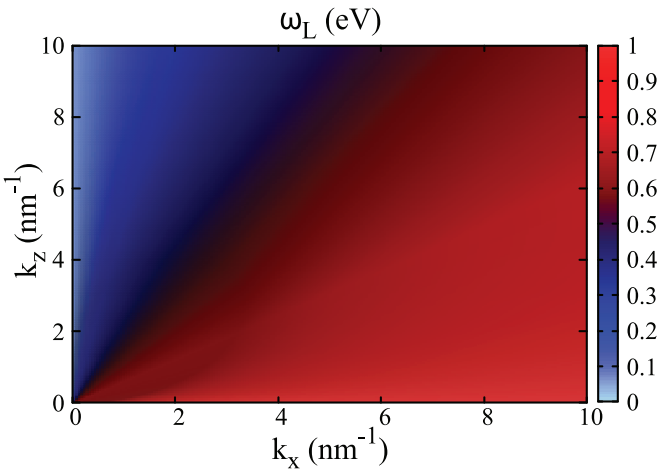

FIG. 2. (a) Plasmon dispersion given by Eq. (31), as obtained by ignoring the coupling of the SC phase to the transverse vector potential. As explained in the text, it also corresponds to the standard result obtained by computing the density-density response in RPA in an anisotropic superconductor [10–13,20,30] or in a metal [31–34]. In such approximation, the polarization of this mode is always longitudinal, so, e.g., at $k_z = 0$ the mode is fully polarized in the plane. Selected cuts of ω_L at fixed k_z as a function of k_x are reported in Fig. 1(c).

The plasmon dispersion obtained after analytical continuation from the phase propagator in Eq. (30) in the limit $\alpha \to 0$ is exactly the result Eq. (2), i.e.,

$$\begin{aligned}\omega_L^2(\mathbf{k}) &= \frac{1}{|\mathbf{k}|^2}\left(\omega_{xy}^2 k_{xy}^2 + \omega_z^2 k_z^2\right)\\ &= \omega_{xy}^2 \frac{k_{xy}^2}{|\mathbf{k}|^2} + \omega_z^2 \frac{k_z^2}{|\mathbf{k}|^2}\\ &= \omega_{xy}^2 \sin^2\eta + \omega_z^2 \cos^2\eta, \end{aligned} \tag{31}$$

where η denotes the angle between the $\mathbf{k}$ vector and the z axis. Equation (31) is plotted in Fig. 2 for the values $\omega_{xy} = 1$ eV and $\omega_z = 0.05$ eV, which lead to an anisotropy $\gamma = \omega_{xy}/\omega_z$ comparable to typical values in cuprates. If one retains corrections due to the finite electronic compressibility, i.e., $\alpha \neq 0$ in Eq. (30), the result Eq. (31) acquires an additional dispersion such that $\omega_L^2(\mathbf{k}) = (\omega_{xy}^2 \frac{k_{xy}^2}{|\mathbf{k}|^2} + \omega_z^2 \frac{k_z^2}{|\mathbf{k}|^2})(1 + \alpha|\mathbf{k}^2|)$. In cuprates [26,53], the Thomas-Fermi wave vector is $k_{\rm TF} \sim 10$ nm^{-2}, so from Eq. (20) one can estimate $\alpha \sim 10^{-2}$ nm^2. As a consequence, this term only contributes near the maximum momentum value reported in Fig. 2, while the large variations as a function of the angle η shown in Fig. 2 are already accounted for by the expression Eq. (31). The result Eq. (31) is analogous to the RPA one derived by including *only* the Coulomb potential. This approach, that we will refer to as *standard* RPA in what follows, has been adopted in previous work both in the SC [10–13,20,30] and in the normal [31–34] state. Within this scheme, it is also possible to generalize the expression Eq. (31) by retaining the lattice periodicity in the z direction [10,13,31–34], and to account for constrained geometries as, e.g., in the transmission through a thin SC slab [42]. The solutions Eq. (31) are sometimes referred to as hyperbolic Josephson plasmons [13,42], since they can be also obtained by the zeros of the anisotropic permittivity for the layered superconductor [13], in analogy with the usual derivation of the solutions for transverse-wave propagation in the so-called hyperbolic materials, i.e., systems where the permittivity has different signs along different crystallographic axis [54,55]. Hyperbolic modes play a crucial role in the case, e.g., of thin SC slabs, since they identify modes propagating in the thin film but decaying exponentially in the surrounding dielectrics [13,42].

As noted in the Introduction, the expression Eq. (31) has a singular limit at $\mathbf{k} = \mathbf{0}$, since its value depends on the angle η. As we shall see below, such a singularity is removed by inclusion of the coupling of the phase to the vector potential $\mathbf{A}$. Finally, for the sake of the following discussion, let us also write explicitly the transverse mode obtained in the same approximation, where one neglects the coupling between $\mathbf{A}_T$ and θ. In this case, assuming, e.g., that the propagating vector is in the xz plane, and choosing the Coulomb gauge such that $\mathbf{k}\cdot\mathbf{A} = k_x A_x + k_z A_z = 0$, one easily finds from the $\mathbf{A}^2$ terms of Eq. (27) two transverse modes, one along y with the standard dispersion $\omega^2 = \omega_{xy}^2 + \tilde{c}^2|\mathbf{k}|^2$ and the other one in the xz plane with the anisotropic dispersion

$$\omega_T^2(\mathbf{k}) \equiv \omega_z^2 \frac{k_{xy}^2}{|\mathbf{k}|^2} + \omega_{xy}^2 \frac{k_z^2}{|\mathbf{k}|^2} + \tilde{c}^2|\mathbf{k}|^2. \tag{32}$$

To fully account for the coupling of the SC phase to both $\mathbf{A}_L$ and $\mathbf{A}_T$, let us take advantage of the results of Sec. II and introduce the g.i. phase variables Eq. (23). To simplify the notation, we can assume without lack of generality that the in-plane momentum is along the x direction. In this case, the ψ_y component decouples from the phase in Eq. (29): It describes a pure massive in-plane transverse mode. The remaining two components are coupled, and with lengthy but straightforward calculations one can derive the generalization of Eq. (25):

$$\begin{aligned} S_{\rm ani}[\boldsymbol{\psi}] = \frac{\varepsilon}{32\pi e^2}\sum_q &\times\Bigg[\left(\frac{1+\alpha k_z^2}{1+\alpha|\mathbf{k}|^2}\Omega_m^2 + \omega_{xy}^2 + \tilde{c}^2 k_z^2\right)|\psi_x(q)|^2\\ &+\left(\frac{1+\alpha k_x^2}{1+\alpha|\mathbf{k}|^2}\Omega_m^2 + \omega_z^2 + \tilde{c}^2 k_x^2\right)|\psi_z(q)|^2\\ &-\left(\frac{\alpha\Omega_m^2}{1+\alpha|\mathbf{k}|^2} + \tilde{c}^2\right)k_x k_z(\psi_x(q)\psi_z(-q) + \text{c.c.})\\ &+\left(\Omega_m^2 + \omega_{xy}^2 + \tilde{c}^2|\mathbf{k}|^2\right)|\psi_y(q)|^2\Bigg]. \end{aligned} \tag{33}$$

We can now compute the propagators $\langle\psi_\alpha(q)\psi_\beta(-q)\rangle$, whose poles identify the collective-mode excitations. From $\langle|\psi_y(q)|^2\rangle$, one immediately finds the dispersion of the massive in-plane transverse mode $\omega^2 = \omega_{xy}^2 + \tilde{c}^2|\mathbf{k}|^2$ that simply reflects the standard isotropic-case result Eq. (15). The fluctuations of ψ_x and ψ_z are coupled, so the collective modes are given by the determinant of their 2×2 matrix, once the analytic continuation $i\Omega_m \to \omega + i0^+$ has been performed. The dispersion of the collective excitations is then obtained as solutions of a *quartic* characteristic equation, which reads,

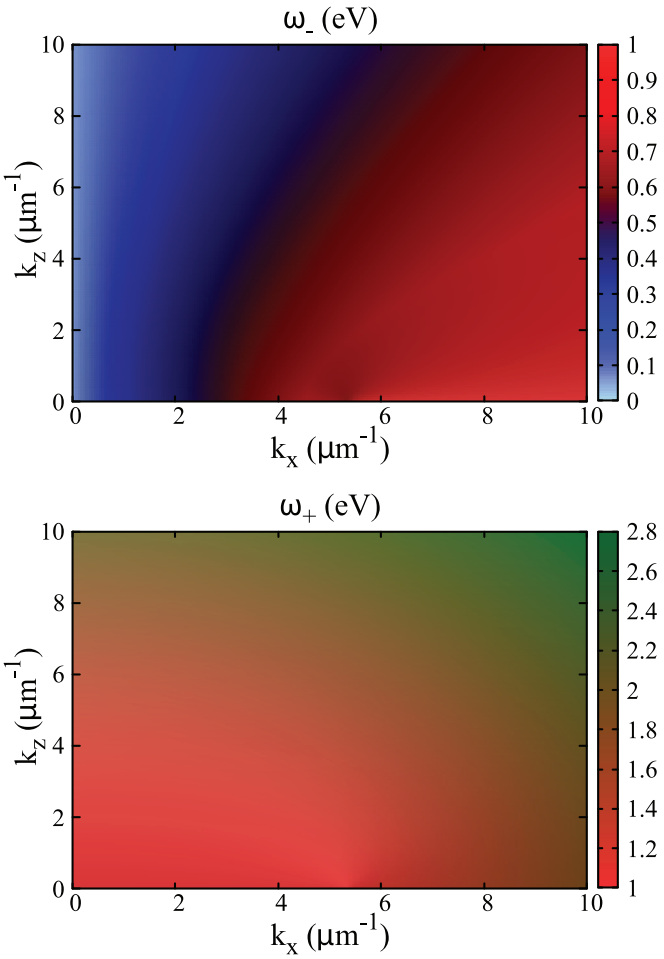

FIG. 3. 2D map of the momentum dependence of the two mixed longitudinal-transverse modes ω_- (top) and ω_+ (bottom) as given by Eq. (35) in the low-momentum regime $k < k_c$, where k_c is defined by Eq. (38). As shown in Fig. 5(a) below and detailed in Eqs. (43) and (44), in this range of momenta the ω_- mode corresponds to a polarization along z, while ω_+ describes polarization in the plane.

in the $\alpha \simeq 0$ limit:

$$\left(\omega^2 - \omega_{xy}^2\right)\left(\omega^2 - \omega_z^2\right) - \tilde{c}^2 k_x^2\left(\omega^2 - \omega_{xy}^2\right) - \tilde{c}^2 k_z^2\left(\omega^2 - \omega_z^2\right) = 0. \tag{34}$$

The solutions of Eq. (34) are

$$\omega_{+/-}^2(\mathbf{k}) = \frac{1}{2}\left(\omega_{xy}^2 + \omega_z^2 + \tilde{c}^2|\mathbf{k}|^2 \pm \sqrt{\left(\omega_{xy}^2 - \omega_z^2\right)^2 + \tilde{c}^4|\mathbf{k}|^4 - 2\tilde{c}^2\left(k_x^2 - k_z^2\right)\left(\omega_{xy}^2 - \omega_z^2\right)}\right). \tag{35}$$

Equation (35) is the first central result of this paper: it provides the general dispersion of the e.m. excitations of a layered system for any momenta. The two solutions Eq. (35) are shown in Fig. 3 as two-dimensional maps, while in Fig. 4 we report the modes as a function of $|\mathbf{k}|$ for selected value of the angle η that $\mathbf{k}$ forms with the z axis. First, we note that ω_+ and ω_- are regular functions as $\mathbf{k} \to \mathbf{0}$. Indeed, assuming that $\omega_{xy} > \omega_z$, as typically happens in layered materials where planes are weakly coupled, one immediately sees that

$$\omega_+^2(\mathbf{k} \to 0) = \omega_{xy}^2, \quad \omega_-^2(\mathbf{k} \to 0) = \omega_z^2, \tag{36}$$

regardless of the direction along which such limit is taken, as is better shown in Fig. 4. At finite $\mathbf{k}$, both solutions give an increasing value of the plasma excitation that is limited above by ω_{xy} for the ω_- solution, while it increases rapidly for the ω_+ solution. Such behavior can be better understood in Fig. 4, where we plot for comparison also the standard RPA results ω_L^2 and ω_T^2 derived neglecting the coupling of the phase to the transverse field, see Eqs. (31) and (32), respectively. Indeed, as $|\mathbf{k}|$ increases the two solutions Eq. (35) reduce to

$$\omega_-(\mathbf{k}) \simeq \omega_L(\mathbf{k}) \qquad \omega_+(\mathbf{k}) \simeq \omega_T(\mathbf{k}). \tag{37}$$

By closer inspection of Eq. (35), one sees that the crossover among the two regimes occurs around a critical value k_c of the momentum set by the ratio between the plasma-frequency anisotropy and the light velocity:

$$k_c = \frac{\sqrt{\omega_{xy}^2 - \omega_z^2}}{\tilde{c}}. \tag{38}$$

Indeed, as soon as $k \gg k_c$ the square-root term in Eq. (35) can be expanded in powers of the small parameter k_c/k and one easily recovers the two analytical expressions of the purely longitudinal and transverse modes ω_L and ω_T, respectively. To get an idea on the order of magnitude of the momentum scale Eq. (38), one should consider that $\hbar c \simeq 0.19$ eVμm. Thus, considering that in layered materials as, e.g., cuprates, it is usually $\omega_z \ll \omega_{xy}$, with $\omega_{xy} \simeq 1$ eV, one sees that as soon as $k \gtrsim k_c \sim 5\,\mu\text{m}^{-1}$ the standard RPA result Eq. (31) is recovered, as shown in Fig. 4. Note that at wave vectors of order of k_c, the term $\alpha|\mathbf{k}^2|$ for the estimated value [26,53] $\alpha \sim 10$ nm^2 in cuprates is quantitatively irrelevant, so the contribution of $\alpha|\mathbf{k}^2|$ corrections can be neglected. As a consequence, ω_- approaches the RPA result Eq. (31) computed at $\alpha = 0$, that is, a constant for a fixed value of the angle η, as shown in Fig. 4. For experiments like EELS or RIXS, which measure the plasma dispersion at momenta of the order of $1/a \sim 0.1$ Å^{-1}, with a lattice spacing, and energies of the order of the eV, the mixing between longitudinal and transverse modes is not quantitatively relevant. Nonetheless, the discrepancy between ω_- and ω_L becomes crucial to understand the radically different description of the low-energy plasma mode provided within the context of nonlinear Josephson plasmonic [14,15]. These experiments are carried out with THz radiation approximately resonant with the low-energy mode $\omega \simeq \omega_z$ and which, at the boundary with the medium, is polarized along the z axis. If one considers the solution of Eq. (34) for $\omega \simeq \omega_z$, one can approximate $\omega^2 - \omega_{xy}^2 \simeq -\omega_{xy}^2$ since $\omega_{xy} \gg \omega_z$. Physically, this is equivalent to neglect the $(\partial\psi_x/\partial\tau)^2$ term in the first line of Eq. (33) with respect to the $\omega_{xy}^2\psi_x^2$ term, i.e., to assume a stationary in-plane current that can be a reasonable approximation at the frequency scale of the soft Josephson plasmon. From the point of view of the eigenmodes of Eq. (33), this approximation turns the quartic Eq. (34) into a quadratic one that can be easily solved leading to Eq. (1) mentioned in the Introduction, that we can also

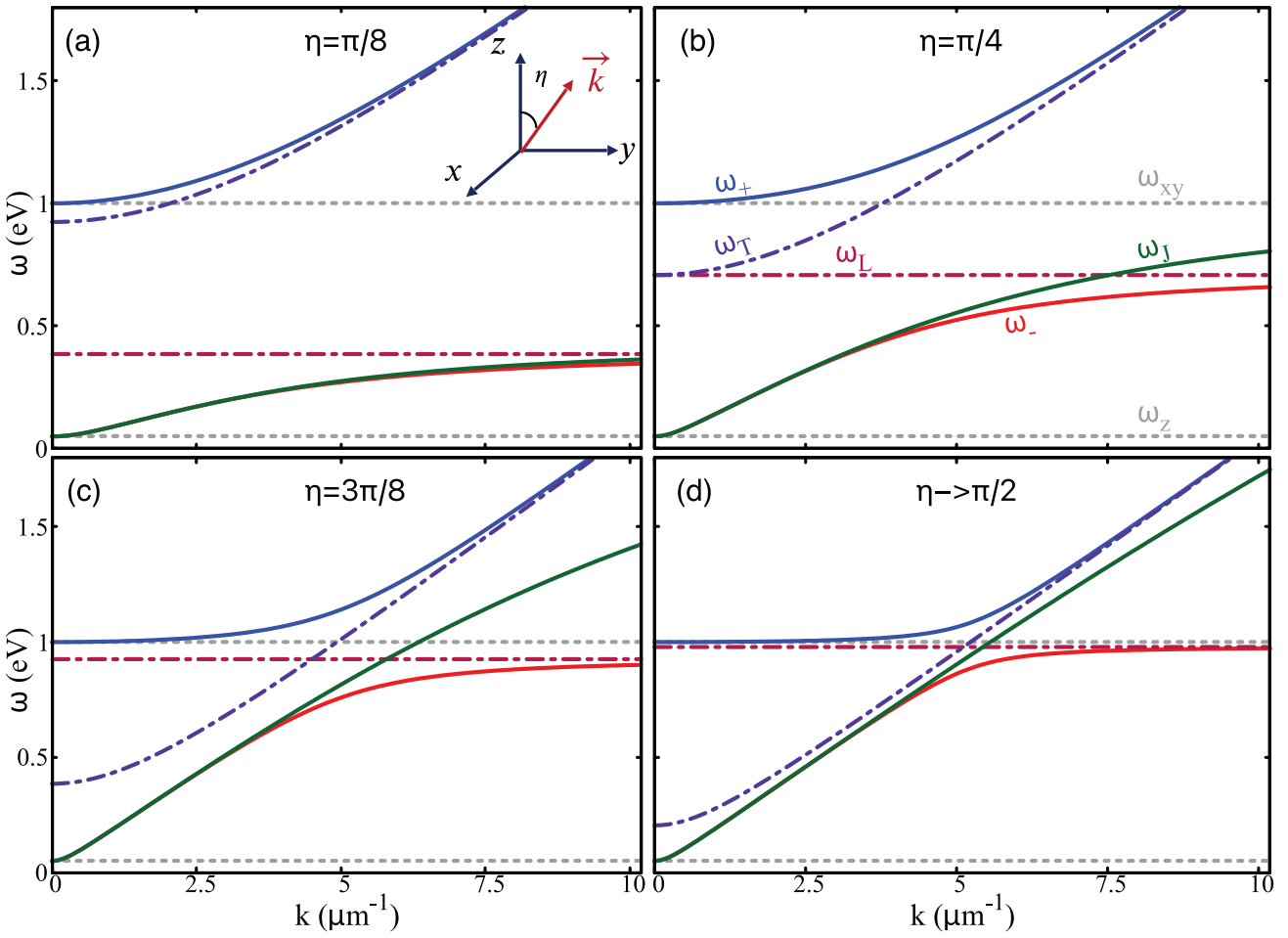

FIG. 4. Momentum dependence of the mixed longitudinal-transverse modes ω_-, ω_+ (red and blue solid lines, respectively) as a function of $|\mathbf{k}|$ at selected value of the angle η between $\mathbf{k}$ and the z axis [see inset of (a)]. We also show for comparison the standard RPA result for the longitudinal ω_L (dot-dashed dark red) and transverse ω_T (dot-dashed dark blue) modes, as given by Eqs. (31) and (32), respectively, and the approximated expression Eq. (39) (green solid line) for ω_J valid around ω_z. Dashed grey lines denote the values of the in-plane ω_{xy} and out-of-plane ω_z plasma modes at zero momentum. As before we set $\omega_{xy} = 1.0$ eV and $\omega_z = 0.05$ eV and for simplicity we assumed $\epsilon = 1$.

rewrite as

$$\omega_J^2 = \omega_z^2\left(1 + \frac{\lambda_z^2 k_x^2}{1 + \lambda_{xy}^2 k_z^2}\right), \tag{39}$$

where we introduced the in-plane and out-of-plane penetration depths:

$$\lambda_{xy/z} \equiv \frac{\tilde{c}}{\omega_{xy/z}}. \tag{40}$$

As shown in Fig. 4, Eq. (39) accounts indeed for the correct behavior of ω_- at energies around ω_z and small momenta. It should be noted that for optical THz probes the relevant value of the momentum $\mathbf{k}$ in Eq. (39) is of the order of 10 to 100 cm^{-1}, so well below the threshold Eq. (38), i.e., in the region where the standard RPA approximation fails. This explains the apparent disagreement between the two expressions usually quoted in the literature for the same problem, studied within the context of different experimental probes.

B. Longitudinal-transverse mixing at generic wave vector

To gain further insight in the mechanism connecting the general solutions $\omega_\pm$ to the results obtained with the standard RPA approximation, it is instructive to express the previous results by introducing explicitly the basis spanned by the longitudinal versor $\hat{\mathbf{k}}$ and by the transverse versors $\hat{\mathbf{y}}$ and $\hat{\mathbf{k}} \times \hat{\mathbf{y}}$. In particular, since we are assuming that $\mathbf{k}$ lies in the xz plane, $\hat{\mathbf{k}}$ denotes the direction of the longitudinal standard RPA plasmon $\omega_L(\mathbf{k})$ of Eq. (31), and $\hat{\mathbf{k}} \times \hat{\mathbf{y}}$ the one of the standard RPA pure transverse mode $\omega_T(\mathbf{k})$ in Eq. (32). By using the rotation matrix among the two basis, which reads

$$\hat{U}(q) = \frac{1}{|\mathbf{k}|}\begin{pmatrix} k_x & 0 & k_z \\ 0 & 1 & 0 \\ -k_z & 0 & k_x \end{pmatrix}, \tag{41}$$

we can rotate the 3×3 matrix associated with the action Eq. (33), which is written in Cartesian basis, into the longitudinal-transverse basis. The resulting action will then

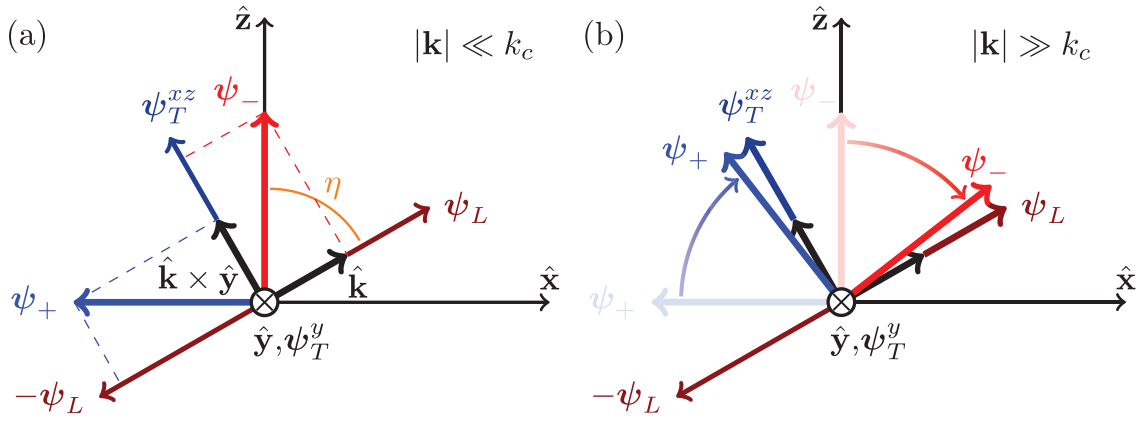

FIG. 5. Sketch of the polarization dependence of the mixed modes in a layered superconductors. Polarization dependence of the solutions ω_- and ω_+ as given by Eq. (44) at generic momentum. The black arrows denote $\hat{\mathbf{k}}$ and the transverse in-plane direction $\hat{\mathbf{k}} \times \hat{\mathbf{y}}$. The orange arc denotes the angle η between the z axis and direction $\hat{\mathbf{k}}$. The longitudinal component $\boldsymbol{\psi}_L$ (polarized along $\hat{\mathbf{k}}$) and the transverse in-plane component $\boldsymbol{\psi}_T^{xz}$ (polarized along $\hat{\mathbf{k}} \times \hat{\mathbf{y}}$) of the g.i. phase difference are, respectively, the dark red and dark blue arrows, while the mixed longitudinal-transverse modes $\boldsymbol{\psi}_-$ and $\boldsymbol{\psi}_+$ are the red and blue arrows. (a) Low-momentum regime $|\mathbf{k}| \ll k_c$. Here the $\boldsymbol{\psi}_\mp$ modes are aligned along the z and x axis, respectively, so at generic $\mathbf{k}$ they are neither pure longitudinal nor pure transverse. (b) Large-momentum regime $|\mathbf{k}| \gg k_c$. Here the mixed mode $\boldsymbol{\psi}_-$ reduces to the pure longitudinal mode $\boldsymbol{\psi}_L$, while $\boldsymbol{\psi}_+$ reduces to the pure transverse mode $\boldsymbol{\psi}_T$. The pure transverse mode $\boldsymbol{\psi}_T^y$, polarised along the y axis, does not get coupled with the other two degrees of freedom in both cases.

read, in the $\alpha \simeq 0$ limit,

$$\begin{aligned} S_{\rm ani}[\boldsymbol{\psi}] = \frac{\varepsilon}{32\pi e^2} \sum_q \big[&\big(\Omega_m^2 + \omega_L^2(\mathbf{k})\big)|\boldsymbol{\psi}_L(q)|^2 \\ &+ \big(\Omega_m^2 + \omega_T^2(\mathbf{k})\big)|\boldsymbol{\psi}_T^{xz}(q)|^2 \\ &- \left(\frac{\omega_{xy}^2 - \omega_z^2}{\tilde{c}^2|\mathbf{k}|^2}\right)\tilde{c}^2 k_x k_z (\psi_L(q)\psi_T^{xz}(-q) + \text{c.c.}) \\ &+ \big(\Omega_m^2 + \omega_{xy}^2 + \tilde{c}^2|\mathbf{k}|^2\big)|\boldsymbol{\psi}_T^y(q)|^2 \big], \end{aligned} \tag{42}$$

where $\boldsymbol{\psi}_T^{xz}$ is the transverse component along $\hat{\mathbf{k}} \times \hat{\mathbf{y}}$. In such a basis, one immediately sees that if the coupling between $\boldsymbol{\psi}_L$ and $\boldsymbol{\psi}_T^{xz}$ is negligible, the action Eq. (42) reduces to the one for the standard RPA modes Eqs. (31) and (32). Whether the coupling term is negligible or not depends on the overall adimensional factor $\frac{\omega_{xy}^2 - \omega_z^2}{\tilde{c}^2|\mathbf{k}|^2}$ that can be recast in the form $\frac{k_c^2}{|\mathbf{k}|^2}$, where k_c is the crossover value of the momentum introduce in Eq. (38) above. When $k \ll k_c$ one can neglect the longitudinal-transverse coupling and one obtains the standard RPA result. On the other hand, if $|\mathbf{k}| \sim k_c$, relativistic effects come in, one must take into account the longitudinal-transverse coupling and standard RPA result breaks down.

Such a crossover is also evident in the polarization dependence of the $\omega_\pm$ solutions that can be equivalently written in both basis. Let us first analyze the low-momentum limit $\mathbf{k} \to 0$. In this regime, the eigenvectors corresponding to the two solutions $\omega_\pm$ read

$$\begin{aligned} \boldsymbol{\psi}_-(\mathbf{k}) &= \frac{\hat{\mathbf{z}} + \frac{\tilde{c}^2 k_x k_z}{\omega_{xy}^2 - \omega_z^2}\hat{\mathbf{x}}}{\sqrt{1 + \frac{\tilde{c}^4 k_x^2 k_z^2}{(\omega_{xy}^2 - \omega_z^2)^2}}} \\ \boldsymbol{\psi}_+(\mathbf{k}) &= \frac{-\hat{\mathbf{x}} + \frac{\tilde{c}^2 k_x k_z}{\omega_{xy}^2 - \omega_z^2}\hat{\mathbf{z}}}{\sqrt{1 + \frac{\tilde{c}^4 k_x^2 k_z^2}{(\omega_{xy}^2 - \omega_z^2)^2}}}. \end{aligned} \tag{43}$$

As one clearly sees, in the $\mathbf{k} \to \mathbf{0}$ limit the $\boldsymbol{\psi}_-$ solution is always polarized along z, while $\boldsymbol{\psi}_+$ is polarized along x, see Fig. 5(a), explaining why the plasma modes always reduce to the $\omega_{z/xy}$ values, without the continuum of $\mathbf{k} \to 0$ values predicted by the standard RPA, see Fig. 2. On the other hand, this also implies that at small momenta the eigenmodes have a mixture of longitudinal and transverse character. This can be better seen by rewriting the two solutions at arbitrary value of the momentum by using explicitly the longitudinal $\boldsymbol{\psi}_L$ and transverse $\boldsymbol{\psi}_T$ components of the g.i. phase:

$$\begin{aligned} \boldsymbol{\psi}_-(\mathbf{k}) &= \frac{\frac{k_x k_z}{|\mathbf{k}|^2}\big(\omega_{xy}^2 - \omega_z^2\big)\boldsymbol{\psi}_L - \big(\omega_-^2(\mathbf{k}) - \omega_L^2(\mathbf{k})\big)\boldsymbol{\psi}_T^{xz}}{\sqrt{\frac{k_x^2 k_z^2}{|\mathbf{k}|^4}\big(\omega_{xy}^2 - \omega_z^2\big)^2 + \big(\omega_-^2(\mathbf{k}) - \omega_L^2(\mathbf{k})\big)^2}} \\ \boldsymbol{\psi}_+(\mathbf{k}) &= \frac{\frac{k_x k_z}{|\mathbf{k}|^2}\big(\omega_{xy}^2 - \omega_z^2\big)\boldsymbol{\psi}_T^{xz} - (\omega_+(\mathbf{k})^2 - \omega_T(\mathbf{k})^2)\boldsymbol{\psi}_L}{\sqrt{\frac{k_x^2 k_z^2}{|\mathbf{k}|^4}\big(\omega_{xy}^2 - \omega_z^2\big)^2 + \big(\omega_+^2(\mathbf{k}) - \omega_T^2(\mathbf{k})\big)^2}}. \end{aligned} \tag{44}$$

As seen in Eq. (33), the pure transverse mode $\boldsymbol{\psi}_T^y$ is not involved in the mixing. The orthogonality between $\boldsymbol{\psi}_-$ and $\boldsymbol{\psi}_+$ is ensured by the fact that $\omega_+^2(\mathbf{k}) + \omega_-^2(\mathbf{k}) = \omega_L^2(\mathbf{k}) + \omega_T^2(\mathbf{k})$.

Equation (44) highlights how, at generic values of the momentum, ω_+ and ω_- describe two modes with no pure (longitudinal or transverse) character. On the other hand, as soon as $k \gg k_c$ and the modes reach the standard RPA value, see Eq. (37), $\boldsymbol{\psi}_-$ becomes a purely longitudinal mode while $\boldsymbol{\psi}_+$ is a purely transverse one, see Fig. 5(b), consistently with the expectation that the standard RPA approximation leads to pure longitudinal or transverse modes. A remarkable exception to the mixing is provided by the case of propagation completely in plane ($k_z = 0$) or completely out of plane ($k_x = 0$), since in this case the $\psi_x \psi_z$ coupling of Eq. (33) vanishes and one obtains purely longitudinal or transverse modes. For instance, when $k_z = 0$ the momentum is along x, so $\boldsymbol{\psi}_+$, which is also aligned along x [see Eq. (43)], describes a purely longitudinal

mode approaching ω_{xy} as $k_x \to 0$. Conversely, when $k_x = 0$ the momentum is along z, so in this case the longitudinal mode is represented by $\boldsymbol{\psi}_-$, and its dispersion approaches ω_z as $k_z \to 0$.

C. Comparison with the sine-Gordon equations of motion

As mentioned in the Introduction, the approximated expression Eq. (39) for the small k limit of ω_- has been widely used in the recent literature [14,15,28] to study the dynamics of the Josephson plasmon in the presence of nonlinear effects due to intense THz fields. Within this context, the equation of motion has been derived for the g.i. variable ψ_z of Eq. (7). The basic equation reads

$$\left(1-\lambda_{xy}^2\frac{\partial^2}{\partial z^2}\right)\left(\frac{1}{\omega_z^2}\frac{\partial^2\psi_z}{\partial t^2}+\sin\psi_z\right)-\lambda_z^2\frac{\partial^2\psi_z}{\partial x^2}=0, \quad (45)$$

where absence of dissipation is assumed for the sake of simplicity. The explicit appearance of the $\sin\psi_z$ term makes the equation nonlinear. As mentioned above, this result shows how the use of the g.i. phase variable represents a powerful and elegant way to obtain a straightforward extension of the Gaussian model to the nonlinear Josephson model that represents a crucial step to describe nonlinear optical effects. On the other hand, the linearized version of Eq. (45), obtained when $\sin\psi_z \simeq \psi_z$, admits a wavelike solution $\psi_z \propto e^{i(\omega t-\mathbf{k}\cdot\mathbf{r})}$ such that the frequency ω and the momentum $\mathbf{k}$ satisfy the dispersion relation Eq. (39). As a consequence, in the linear regime, Eq. (45) provides again an approximation for the ω_- solution at low energy and momenta. It is then interesting to understand how such a nonlinear extension to the Josephson model can be obtained starting from the more general formalism developed so far.

A simple way to see the analogy is to rewrite the general result Eq. (33) in real space. Consistently with the derivation of Eq. (35), we shall consider here the $\alpha = 0$ limit. In addition, since Eq. (45) is written in real time we will convert Matsubara frequencies to real frequencies via analytical continuation and we will replace $\int d\tau = \int idt$. The resulting real-time action $\tilde{S}_{\rm ani}$ then reads

$$\begin{aligned}\tilde{S}_{\rm ani}[\psi] = \frac{\varepsilon}{32\pi e^2}\int dt d\mathbf{x}\Bigg\{&\left(\frac{\partial\psi_x}{\partial t}\right)^2+\left(\frac{\partial\psi_z}{\partial t}\right)^2\\ &-\omega_{xy}^2\psi_x^2-\tilde{c}^2\left(\frac{\partial\psi_x}{\partial z}\right)^2\\ &+2\omega_z^2\cos(\psi_z)-\tilde{c}^2\left(\frac{\partial\psi_z}{\partial x}\right)^2\\ &-\tilde{c}^2\left[\psi_x\frac{\partial^2\psi_z}{\partial x\partial z}+\psi_z\frac{\partial^2\psi_x}{\partial x\partial z}\right]\Bigg\}. \end{aligned} \quad (46)$$

Notice that we promoted the $\omega_z^2\psi_z^2$ term of Eq. (33) to a cosine-like term $-2\omega_z^2\cos\psi_z$, so interacting terms for the phase are included beyond the Gaussian order. As usual, this is physically motivated by the idea that a Josephson-like coupling set by the out-of-plane phase stiffness D_z exists for the phase in neighboring layers, leading to an effective XY model for the phase degrees of freedom. The main consequence of the presence of a cosine term is that the resulting phase-only model admits naturally a nonlinear current along the z direction, $I_z \propto \omega_z \sin\psi_z$, that is crucial to account for the nonlinear optical response measured at strong THz fields aligned along the z direction in cuprates [35,36]. As discussed in Ref. [12], the interacting terms for the phase derived microscopically can differ from the one obtained within the simple XY model. Nonetheless, the XY model provides a reasonable starting point to account for nonlinear effects in the z direction, as discussed recently in Ref. [40]. Finally, to account for the layered structure the g.i. phase variable $\boldsymbol{\psi}$ should be promoted to a layer-dependent variable $\boldsymbol{\psi}(\mathbf{r}, z = nd) \to \boldsymbol{\psi}_n(\mathbf{r}, t)$, with $\mathbf{r} = (x, y)$, n layer index and d spacing between layers. The final result is completely analogous to Eq. (46), provided that one discretizes the integration along z as $\int d\mathbf{x} \to d\sum_n \int d\mathbf{r}$ and defines a discrete version of the derivative along the z direction, so $\partial_z f \equiv \frac{1}{d}\partial_n f = \frac{f_{n+1}-f_n}{d}$. We will then retain for simplicity the continuous notation in what follows.

Once rewritten in the action in real space, we can obtain the Euler-Lagrange equations of motion by functional derivatives with respect to ψ_x and ψ_z. By simple algebra, we then obtain two coupled equations which describe the dynamics of the mixed longitudinal-transverse modes:

$$\frac{\partial^2\psi_x}{\partial t^2}+\omega_{xy}^2\psi_x-\tilde{c}^2\frac{\partial^2\psi_x}{\partial z^2}+\tilde{c}^2\frac{\partial^2\psi_z}{\partial x\partial z}=0, \quad (47)$$

$$\frac{\partial^2\psi_z}{\partial t^2}+\omega_z^2\sin\psi_z-\tilde{c}^2\frac{\partial^2\psi_z}{\partial x^2}+\tilde{c}^2\frac{\partial^2\psi_x}{\partial x\partial z}=0. \quad (48)$$

As one can easily check, when $\sin\psi_z \simeq \psi_z$ one recovers two coupled linear equations which can be solved with wavelike solutions propagating with frequency ω and momenta $\mathbf{k}$ satisfying the same Eq. (34) derived above. Thus, in the linear regime, as expected, one recovers the same expression Eq. (35) for the $\omega_\pm$ collective modes derived by the Gaussian action Eq. (33). On the other hand, if one is interested in studying the collective dynamics of ψ_z for frequencies around ω_z, one can get an approximate equation of motion by noticing that for $\omega \simeq \omega_z \ll \omega_{xy}$ the first time-derivative term of Eq. (47) is of order $(\omega_z/\omega_{xy})^2$ as compared to the second one, and can then be neglected. Thus one simply deduces from Eq. (47) that

$$\left(1-\lambda_{xy}^2\partial_z^2\right)\psi_x = -\lambda_{xy}^2(\partial_x\partial_z)\psi_z, \quad (49)$$

where we introduced the penetration depths Eq. (40). By applying the $(1-\lambda_{xy}^2\partial_z^2)$ operator to Eq. (48) and using Eq. (49), one obtains exactly Eq. (45). In this way, we reconciled all the expressions discussed in previous literature by also clarifying the limit of validity of the various approximations.

A last comment is in order about the role of the $\alpha|\mathbf{k}|^2$ terms, neglected while deriving the $\omega_\pm$ expressions in Eq. (35). In the isotropic case, these terms are crucial to get the plasmon dispersion, see Eq. (22). Since $\alpha = \lambda_D^2$ coincides with the Debye length squared, see Eq. (20), its effect is negligible as compared to the much larger variations in $\mathbf{k}$ between ω_z and ω_{xy} already described by Eq. (35). On the other hand, including these corrections into the general solutions $\omega_\pm$ is a matter of simple algebra and, in the standard RPA regime, one would just recover an additional $\alpha|\mathbf{k}|^2$ dispersion into Eq. (31).

IV. GAUGE-INVARIANT DENSITY-DENSITY RESPONSE INCLUDING RELATIVISTIC CORRECTIONS

So far, we have investigated the nature of the mixed longitudinal-transverse mode by looking at the dynamics of the g.i. phase variable, and we showed a failure of the standard RPA approach to capture the $\mathbf{k} \to 0$ limit of the plasma dispersion. It is then worth investigating how such generalized plasma modes appear in the physical g.i. density-density response function, which carries information on the longitudinal degrees of freedom of the system.

To clarify the procedure, we first outline the derivation of the density-density response function for an isotropic SC system. The simplest way is to add an auxiliary scalar field $\delta\phi$ coupled to the density operator into the microscopic Hamiltonian, so the density-density response can be obtained by functional derivative of the total action with respect to $\delta\phi$. In practice, the idea is to derive an action quadratic in $|\delta\phi|^2$ after integration out of all other variables so the density-density response function K will be the coefficient of the $|\delta\phi|^2$ term in the final action, i.e.,

$$K(q) = -\frac{\partial^2 S[\delta\phi]}{\partial\delta\phi(q)\partial\delta\phi(-q)}, \tag{50}$$

where $S[\delta\phi]$ has been obtained by integrating out all other degrees of freedom except the auxiliary field. In the isotropic case, the result is straightforward. Indeed, once known, the phase-only action Eq. (10), the scalar perturbation $\delta\phi$, enters the Gaussian phase-only action via the usual minimal coupling substitution Eq. (12). One is then left with an effective Gaussian model for the variables θ, $\delta\phi$, and ϕ, where the action $S_{\delta\phi}$ adds to the contribution Eq. (24) computed before. The action $S_{\delta\phi}$ contains a bare quadratic term, which accounts for the bare compressibility, and the coupling of the phase with the scalar perturbation. These read

$$S_{\delta\phi}[\delta\phi,\theta] = \sum_q \Big[-\frac{\kappa_0}{2}|\delta\phi(q)|^2 + \frac{\kappa_0}{4}\Omega_m\delta\phi(q)\theta(-q) + \text{H.c.}\Big]. \tag{51}$$

As before, we can introduce the g.i. phase variable $\boldsymbol{\psi}$ and integrate out explicitly θ. This leads to a dressing of the bare compressibility term which multiplies $|\delta\phi(q)|^2$ in Eq. (51) and generates a coupling among $\delta\phi$ and $\boldsymbol{\psi}$:

$$S[\boldsymbol{\psi},\delta\phi] = \sum_q \Bigg\{-\frac{\kappa_0}{2k_{\text{TF}}^2}\frac{|\mathbf{k}|^2}{1+\alpha|\mathbf{k}|^2}|\delta\phi(q)|^2 + \frac{\varepsilon}{32\pi e^2}\left(\frac{\Omega_m^2}{1+\alpha|\mathbf{k}|^2}+\omega_p^2\right)|\boldsymbol{\psi}_L(q)|^2 + \frac{\kappa_0}{4k_{\text{TF}}^2}\frac{i\Omega_m|\mathbf{k}|}{1+\alpha|\mathbf{k}|^2}\delta\phi(q)|\boldsymbol{\psi}_L(-q)| - \text{H.c.}\Bigg\}. \tag{52}$$

As expected, the scalar perturbation couples only to the longitudinal component $\boldsymbol{\psi}_L$ of the g.i. phase difference, carrying the information on the longitudinal modes. Once $\boldsymbol{\psi}_L$ is integrated out, we get the fully dressed density-density response function from Eq. (50). Neglecting the plasmon dispersion (i.e., $\alpha \simeq 0$) and performing the analytic continuation $i\Omega_m \to \omega + i\delta$, it reads

$$K(q) = \frac{\kappa_0}{k_{\text{TF}}^2}\frac{|\mathbf{k}|^2\omega_p^2}{\omega_p^2-(\omega+i\delta)^2}. \tag{53}$$

Equation (53) displays a singularity at the plasma frequency ω_p. One can easily check that Eq. (53) is perfectly equivalent to the standard RPA result $K_{\text{RPA}}(q) = \frac{\chi_0(q)}{1+V_C(\mathbf{k})\chi_0(q)}$ obtained in the normal state [3,6], where $\chi_0(q)$ is the Lindhard function for the metal. Indeed, in the limit $\omega/k \gg 1$ the Lindhard function can be approximated as $\chi_0(q) \simeq -\frac{n}{m}\frac{|\mathbf{k}|^2}{\omega^2}$, which replaced into the standard RPA formula gives exactly Eq. (53). Since in this frequency and momentum regime, one would expect that the SC susceptibility has the same behavior of the normal-state one, one can conclude that Eq. (53) is equivalent to the standard RPA result for the isotropic superconductor. By retaining terms in $\alpha|\mathbf{k}|^2$ in Eq. (52), one could get also the plasmon dispersion. However, the extension of Eq. (53) will not give the correct damping of the plasmon, since it has been derived taking directly the static limit of the density response, i.e., $\kappa_0 = \chi_0(\omega = 0, \mathbf{k} \to 0)$. To get the full plasmon spectral function, one should retain the full frequency and momentum dependence of the bare density-density response χ_0 to recover a plasmon damping when $\omega_p(\mathbf{k})$ overlaps the particle-hole continuum [3,6].

To generalize the previous derivation to the anisotropic case, we should introduce, in full analogy with Sec. III, the in-plane and out-of-plane superfluid stiffness D_{xy} and D_z. This leaves unchanged the coupling between $\delta\phi$ and $\boldsymbol{\psi}_L$ in Eq. (52), but it modifies the term in $|\boldsymbol{\psi}_L|^2$. Once again, the standard RPA result does not account for this effect and only introduces the anisotropy of the bare Lindhard function. For an anisotropic metal, this would be equivalent to approximate $\chi_0(q) \simeq -\frac{n}{\omega^2}(\frac{k_x^2}{m_{xy}}+\frac{k_z^2}{m_z})$, where the anisotropic in-plane m_{xy} and out-of-plane m_z masses identify the anisotropic plasma frequencies $\omega_{xy/z}^2 = 4\pi e^2 n/m_{xy/z}$. As a consequence, the standard RPA result for the anisotropic case is fully equivalent to Eq. (53), provided that ω_p^2 is replaced by its layered version ω_L^2 defined in Eq. (31), i.e.,

$$K_{\text{RPA}}^{\text{ani}} = \frac{\kappa_0}{k_{\text{TF}}^2}\frac{|\mathbf{k}|^2\omega_L(\mathbf{k})^2}{\omega_L^2(\mathbf{k})-(\omega+i\delta)^2}. \tag{54}$$

As discussed before, we expect that such an approximation fails in the $k \ll k_c$ regime. Indeed, by extending the procedure outlined above for the isotropic case and by integrating out the longitudinal g.i. component $\boldsymbol{\psi}_L$ at arbitrary momentum we obtain the following generalization of Eq. (53) in the $k \ll k_{\text{TF}}$ limit:

$$K^{(\text{ani})}(q) = \frac{\kappa_0|\mathbf{k}|^2}{k_{\text{TF}}^2}\left(1-\frac{\omega^2\big(\omega^2-\omega_T^2(\mathbf{k})\big)}{[(\omega+i\delta)^2-\omega_-^2(\mathbf{k})][(\omega+i\delta)^2-\omega_+^2(\mathbf{k})]}\right). \tag{55}$$

From Eq. (55), one sees that the poles of $K^{(\text{ani})}$ are the generalized plasma modes ω_+ and ω_- at generic $\mathbf{k}$. This is consistent with the fact that both have a finite longitudinal projection. Also, in this case, the full computation of the density spectral

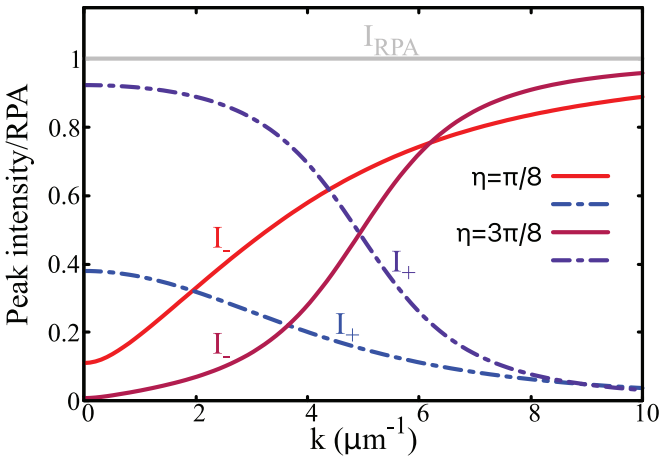

FIG. 6. Momentum dependence of the spectral weights of the $\omega_\pm$ poles in the density-density response. Here we show $I_\pm$ from Eq. (56) as a function of $|\mathbf{k}|$ for two fixed values of the angle η between $\mathbf{k}$ and the z axis. To compare the results at different angles η, the intensities $I_\pm$ have been normalized to the intensity of the standard RPA longitudinal mode, i.e., $I_{\rm RPA} = \omega_L(\mathbf{k})/2$.

function requires a careful evaluation of its imaginary part that is beyond the scope of the present paper. Nonetheless, the result Eq. (55) already provides us with the direct access to the total spectral weight $I_\pm(\mathbf{k})$ allocated in each $\omega_\pm(\mathbf{k})$ pole as a function of momentum $\mathbf{k}$, as given by the imaginary part of Eq. (55). These can be readily obtained as

$$I_\pm(\mathbf{k}) = \pm \frac{\omega_\pm^2(\mathbf{k})\big(\omega_\pm^2(\mathbf{k}) - \omega_T^2(\mathbf{k})\big)}{2\omega_\pm(\omega_+^2 - \omega_-^2)}. \tag{56}$$

The momentum dependence of $I_\pm(\mathbf{k})$ is shown in Fig. 6 for two values of angle η between $\mathbf{k}$ and the z axis, corresponding to Figs. 4(a) and 4(c). Note that to compare the relative spectral weights at a fixed $\mathbf{k}$, we did not include in Eq. (56) the overall $|\mathbf{k}|^2$ factor present in the density-density response Eq. (55). As a consequence, in the $k \ll k_c$ regime where the $\omega_\pm$ solutions are different from the standard RPA ones $\omega_{T/L}$, the upper pole at ω_+ always has a larger spectral weight than the lower one, ω_-, due to the overall ω^2 factor in Eq. (55). Conversely, in the $k \gg k_c$ limit, where ω_- reduces to the pure RPA longitudinal mode and ω_+ to the pure RPA transverse mode [see Eq. (37)] only the lower pole at ω_- survives. Indeed, in this regime one sees from Eq. (56) that the factor $\omega_+^2 - \omega_T^2$ in the numerator of I_+ vanishes, while the factor $\omega_-^2 - \omega_+^2 \simeq \omega_-^2 - \omega_T^2$ at the denominator of I_- cancels out exactly the weighting factor $\omega_-^2 - \omega_T^2$ in the numerator, so I_- approaches the spectral weight of the standard RPA longitudinal mode, which is defined from Eq. (54) as $I_{\rm RPA} = \omega_L(\mathbf{k})/2$. In other words, in this regime the density-density response approaches $K_{\rm RPA}^{\rm ani}$ in Eq. (54), obtained in the standard RPA approach. Conversely, at $k \ll k_c$, Eq. (55) represents a rather unexpected result, i.e., the simultaneous signature in the density response of two generalized plasma modes, located at two well-separated energy scales, with the initial predominance of the higher-energy solution ω_+.

V. CONCLUSIONS

In the present paper, we provided the full description of the generalized plasma modes in bulk layered superconductors, filling the knowledge gap among previous results that focused on specific regions of the energy and momentum spectrum of the plasmons. The main physical mechanism behind our findings is the anisotropy of the superfluid response in layered superconductors that leads to an induced superfluid current which is no more parallel to the electric field. As already evident at the level of classical Maxwell's equations (Appendix B), this induces a mixing between transverse and longitudinal components of the e.m. fields, usually absent in isotropic systems. To rephrase the same effect in another way, in the anisotropic system density fluctuations are not only generated by a scalar potential but also by a vector potential, and within the context of the superconductor it appears as a finite coupling of the SC phase to the transverse vector potential. Such effects become typically relevant for wave vectors that, in strongly anisotropic systems (where i.e., $\omega_{xy} \gg \omega_z$), are smaller than $k_c \sim \omega_{xy}/c$. Since this scales vanishes as $c \to \infty$, these effects appear as relativistic corrections. At momenta well above the crossover scale, the modes acquire an almost pure longitudinal or transverse character and the anisotropy only manifests in the emergence of acousticlike plasmon branches reminiscent of the plasma modes in purely 2D systems. A remarkable exception to the mixing occurs when light propagates purely in plane or out of plane, since in this case one can gauge away the coupling to the vector potential and the standard RPA approach gives back the exact solution.

The above results have been derived by taking advantage of the fact that in a superconductor the plasma modes can be conveniently studied by means of the dynamics of the SC phase of the order parameter. However, previous approaches focused on apparently different models, making it difficult to establish a link between the different expressions for the plasma dispersion discussed in the literature. In contrast, our approach incorporates in an elegant and general way the mixing among transverse and longitudinal response, previously discussed for the low-momenta regime [25–27,29,39,41], and allows one to understand why it becomes irrelevant in the nonrelativistic regime at large momentum, where a standard RPA result [10–13,20,30] is recovered. Taking advantage of this description, we derive an analytical expression for two hybrid light-matter modes valid at all momenta, providing a viable tool for a direct comparison with experiments that goes beyond numerical solutions of coupled light-matter equations [39,41]. In addition, we explain how to extend the description to incorporate nonlinear effects relevant for THz spectroscopy at strong field [15,35–38] and we explicitly compute the density-density response, showing how the generalized hybrid modes are projected out in the physical response in the various energy and momentum regimes.

Our results, including the methodological aspects, are particularly relevant for future work aimed at investigating, e.g., the plasma modes in confined geometries, as is the case for surface plasmon polaritions [4,5,42]. The recent detection of surface Josephson plasma waves in an ultrathin film of the high-temperature superconductor $La_{1.85}Sr_{0.15}CuO_4$ shows

that the field is now mature to apply near-field optics, efficiently used so far to investigate van der Waals layered metals [5], to layered superconductors. At the same time, even if standard EELS or RIXS experiments have a rather low-momentum resolution, with the lowest accessible momenta of about ∼0.1 of the reciprocal lattice unit, EELS incorporated in a scanning transmission electron microscope (STEM-EELS) and equipped with a monochromator and aberration correctors has a high potential to combine high spatial and energy resolution [56,57]. As a consequence, one can hope in the near future to be able to probe plasma excitations around the crossover scale $k_c \sim 50\,\mu\text{m}^{-1}$, where approximate solutions fail, and where both generalized plasma modes give a comparable contribution to the density response, as we showed in Sec. IV. In addition, at these wave vectors and energies one could explore the possible coupling with other collective modes like phonon, giving rise to hybrid phonon-polaritons modes [4], involving simultaneously transverse and longitudinal fields. As a final remark, it could be interesting to explore how the transverse-longitudinal mixing affects the plasmon dispersion in the normal state, even though in this case the soft Josephson plasmon is expected to be strongly overdamped by the quasiparticle continuum, especially in correlated systems like cuprates. Indeed, it is worth noting that even though our results have been derived in the SC state, we expect a similar physics to be at play also in the normal state at scales sufficiently larger than twice the SC gap, where the effects of the gap opening are no more visible, making it irrelevant possible heating effects due to a probing frequency of the order of ω_{xy}. A detailed analysis of the generalized plasma wave in the layered metal and in correlated systems like cuprates will be deserved for future work. Such analysis can also help understanding how to model the Coulomb interaction among the scattered electrons and the local density of the layered metal in EELS experiments in cuprates, whose interpretation is still debated [48–51]. Indeed, a robust modeling of the plasma modes in conventional layered superconductors and metals is certainly a prerequisite in order to understand how charge fluctuations manifest instead in a correlated system like cuprates.

ACKNOWLEDGMENTS

We acknowledge financial support by EU under project MORE-TEM ERC-SYN (Grant Agreement No 951215).

APPENDIX A: PHASE-ONLY EFFECTIVE ACTION IN THE PATH-INTEGRAL FORMALISM

We model a generic single-band superconductor via the following grand-canonical Hamiltonian:

$$\hat{H} - \mu\hat{N} = \sum_{\mathbf{k},\sigma} \xi_{\mathbf{k}} \hat{c}^{+}_{\mathbf{k}\sigma} \hat{c}_{\mathbf{k}\sigma} + \hat{H}_I, \tag{A1}$$

where $\xi_{\mathbf{k}}$ is the band dispersion with respect to the chemical potential μ, and the interacting Hamiltonian $\hat{H}_I$ reads

$$\hat{H}_I = -\frac{U}{N} \sum_{\mathbf{q}} \hat{\Phi}^{+}_{\Delta}(\mathbf{q}) \hat{\Phi}_{\Delta}(\mathbf{q}); \tag{A2}$$

$\hat{\Phi}_{\Delta}(\mathbf{q}) \equiv \sum_{\mathbf{k}\sigma} \hat{c}^{+}_{\mathbf{k}-\mathbf{q}/2\sigma} \hat{c}_{\mathbf{k}+\mathbf{q}/2,\sigma}$ being the pairing operator, $U > 0$ being the SC coupling constant, and N denotes the number of lattice sites. To compute thermal averages over the Hamiltonian Eq. (A1), we use the path integral formulation. Within such framework, the the partition function of the system is given by $\mathcal{Z} = \int \mathcal{D}[c, \bar{c}] e^{-S[c,\bar{c}]}$, where S is the imaginary-time action for fermions [6]:

$$\begin{aligned} S[c, \bar{c}] &= S_0 + S_I \\ &= \int_0^{\beta} d\tau \left[\sum_{\mathbf{k}\sigma} \bar{c}_{\mathbf{k}\sigma} (\partial_\tau + \xi_{\mathbf{k}}) + H_I(\tau) \right]. \end{aligned} \tag{A3}$$

$\tau = it$ is the imaginary time, $\beta = \frac{1}{T}$ and c, $\bar{c}$ are the Grassmann variables associated to the annihilation and creation operators, respectively. To obtain the effective action in terms of the order-parameter collective degrees of freedom, the interacting action is decoupled in the particle-particle channel by means of the HS transformation by introducing the auxiliary complex field Δ:

$$\Delta(\mathbf{r}) = (\Delta_0 + \delta\Delta(\mathbf{r})) e^{\theta(\mathbf{r})}, \tag{A4}$$

where Δ_0 is the mean-field expectation value of the amplitude associated to the SC energy gap, $\delta\Delta$ and θ are amplitude and phase fluctuations. By making an appropriate gauge transformation on the Grassmann fields c and $\bar{c}$, it is possible to make the dependence on phase θ explicit in the action. One then finds that the HS transform of S_I is phase independent, while the free contribution S_0 becomes

$$\tilde{S}_0 = S_{\text{BCS}} + \int d\mathbf{x} d\tau \overline{\Psi}(\mathbf{x}, \tau) \hat{\Sigma}(\mathbf{x}, \tau) \Psi(\mathbf{x}, \tau), \tag{A5}$$

where Ψ is the Nambu spinor, defined as the column vector $(c_\uparrow, c_\downarrow)$, and S_{BCS} is the BCS saddle-point action, where only the mean-field value Δ_0 is the complex field has been included, while fluctuations are contained in $\hat{\Sigma}$. The BCS Green's functions are defined from S_{BCS} as

$$\begin{aligned} \mathcal{G}_0(\mathbf{k}, i\omega_m) &\equiv -\int_0^{\beta} d\tau \left\langle \mathcal{T}\left(\hat{\Psi}_{\mathbf{k}}(\tau) \hat{\Psi}_{\mathbf{k}}(0)\right)\right\rangle e^{i\omega_m \tau}; \\ &= \frac{i\omega_m \hat{\tau}_0 + \xi_{\mathbf{k}} \hat{\tau}_3 - \Delta_0 \hat{\tau}_1}{(i\omega_m)^2 - E^2_{\mathbf{k}}}; \end{aligned} \tag{A6}$$

$i\omega_m = (2n+1)\pi T$ being Matsubara fermionic frequencies, $E_{\mathbf{k}} = \sqrt{\xi^2_{\mathbf{k}} + \Delta^2_0}$ being the quasiparticle energy, $\hat{\tau}_i$ being the Pauli matrices. $\hat{\Sigma}$ is the self-energy, which depends, in principle, on both amplitude and phase fluctuations. Nonetheless, as long as one is interested in the low-temperature dynamics of phase fluctuations in layered cuprates, amplitude fluctuations can be neglected [12]. The self-energy then reads

$$\hat{\Sigma} = \left\{ \frac{i}{2} \partial_\tau \theta + \frac{1}{8m} (\nabla\theta)^2 \right\} \hat{\tau}_3 + \left\{ \frac{i}{4m} \nabla\theta \cdot \overleftrightarrow{\nabla} \right\} \hat{\tau}_0, \tag{A7}$$

where $\overleftrightarrow{\nabla} \equiv \overrightarrow{\nabla} - \overleftarrow{\nabla}$. Note that, according to Goldstone theorem, phase θ appears only trough its time and spatial derivatives in Eq. (A7), i.e., no mass term for θ is allowed. Now, since the fermionic variables appear quadratically into $\tilde{S}_0$, one can integrate them out. Such procedure leads to the

following effective action for phase fluctuations:

$$S_{\rm eff}[\theta] = \frac{1}{n}\sum_{n=1}^{+\infty} {\rm Tr}\{(\hat{\mathcal{G}}_0\hat{\Sigma})^n\}, \tag{A8}$$

where the trace is computed over both spin and momentum degrees of freedom. To study the phase dynamics, we compute the effective action at a Gaussian level, i.e., by including terms up to $n = 2$. It reads, in Fourier space,

$$S_G[\theta] = \frac{1}{8}\sum_q \big[\Omega_m^2\Lambda_{\rho\rho}(q) - \mathbf{q}_a\mathbf{q}_b\Lambda_{JJ}^{(ab)} + 2i\Omega_m\mathbf{q}_a\Lambda_{\rho J}^{(a)}\big]|\theta(q)|^2, \tag{A9}$$

where $q \equiv (i\Omega_m, \mathbf{q})$, $\Omega_m = 2\pi mT$ being a bosonic Matsubara frequency, and

$$\Lambda_{\rho\rho}(q) \equiv \frac{T}{N}\sum_k {\rm tr}\{\hat{\mathcal{G}}_0(k+q)\hat{\tau}_3\hat{\mathcal{G}}_0(k)\hat{\tau}_3\}, \tag{A10}$$

$$\Lambda_{\rho J}^{a}(q) \equiv \frac{T}{N}\sum_k \frac{\mathbf{k}_a + \frac{\mathbf{q}_a}{2}}{m}{\rm tr}\{\hat{\mathcal{G}}_0(k+q)\hat{\tau}_0\hat{\mathcal{G}}_0(k)\hat{\tau}_3\}, \tag{A11}$$

$$\Lambda_{JJ}^{ab}(q) \equiv -\frac{n}{m}\delta_{ab} + \frac{T}{N}\sum_k \frac{\mathbf{k}_a + \frac{\mathbf{q}_a}{2}}{m}\frac{\mathbf{k}_b + \frac{\mathbf{q}_b}{2}}{m}{\rm tr}\{\hat{\mathcal{G}}_0(k+q)\hat{\tau}_0\hat{\mathcal{G}}_0(k)\hat{\tau}_0\} \tag{A12}$$

are the BCS response functions, which contain all the information on the microscopic fermionic degrees of freedom. Again, if one is interested in the low-temperature phase dynamics, the *hydrodynamic limit* of the Gaussian action Eq. (A9) is the relevant one. Within such approximation, the BCS bubbles are computed in the static limit $i\Omega_m = 0, \mathbf{q} \to \mathbf{0}$, and one finds Eq. (10) of the main text.

The formalism developed so far is appropriate for describing neutral superfluids. For the case of superconductors, the e.m. interaction between electrons must be taken into account. This can be achieved via the scalar and vector potentials ϕ and $\mathbf{A}$, which account for internal e.m. degrees of freedom. They can be included into the self-energy Eq. (A7) by means of the minimal-coupling substitution, which reads in imaginary time as $\partial_\tau \to \partial_\tau - e\phi$, $-i\boldsymbol{\nabla} \to -i\boldsymbol{\nabla} + \frac{e}{c}\mathbf{A}$ for the fermionic degrees of freedom. After such a procedure, the self-energy Eq. (A7) undergoes the following modification:

$$\hat{\Sigma} = \left\{\frac{1}{2}(i\partial_\tau\theta + 2e\phi) + \frac{1}{8m}\left(\boldsymbol{\nabla}\theta - \frac{2e}{c}\mathbf{A}\right)^2\right\}\hat{\tau}_3 + \left\{\frac{i}{4m}\left(\boldsymbol{\nabla}\theta - \frac{2e}{c}\mathbf{A}\right)\cdot\overleftrightarrow{\nabla}\right\}\hat{\tau}_0. \tag{A13}$$

One immediately sees that Eq. (A13) can be obtained as well by making the substitution Eq. (7) on the phase degrees of freedom. At this point, it is possible to expand the effective action at Gaussian level in both the phase and the e.m. potentials: By doing such a procedure and by adding the free-e.m. contribution Eq. (11), one obtains the total action Eq. (13).

External perturbations can be also introduced to compute the response function of the system. For example, to compute the density-density response function, one can introduce a scalar perturbation $\delta\phi$, which couples with the density operator $\hat{\rho}_{\mathbf{q}} = \sum_{\mathbf{k}\sigma}\hat{c}^+_{\mathbf{k}+\mathbf{q}\sigma}\hat{c}_{\mathbf{k}\sigma}$ into the microscopic Hamiltonian trough the following contribution:

$$\hat{H}_{\delta\phi} = \sum_{\mathbf{q},\mathbf{k}\sigma}\delta\phi(\mathbf{q})\hat{c}^+_{\mathbf{k}+\mathbf{q}\sigma}\hat{c}_{\mathbf{k}\sigma}. \tag{A14}$$

Equation (A14) will give rise to the density insertion $e\delta\phi\hat{\tau}_3$ into the self-energy Eq. (A13). At this point, one can compute, through the usual expansion Eq. (A8), the effective action at Gaussian level in the phase, the internal e.m. degrees of freedom and the scalar perturbation. Then, once the g.i. variable $\boldsymbol{\psi}$ has been introduced and the phase has been integrated out, one is left with Eq. (52), which describes the coupling of the scalar perturbation $\delta\phi$ with the longitudinal degrees of freedom (described by $\boldsymbol{\psi}_L$) of the system.

APPENDIX B: CLASSICAL ELECTRODYNAMICS OF A LAYERED SUPERCONDUCTOR

In this Appendix, we rephrase the main result of this paper, i.e., the existence of mixed longitudinal-transverse e.m. modes in layered superconductors, within the classical framework of Maxwell's equations. A similar approach has been discussed within the context of the soft Josephson plasmon, see, e.g., Refs. [27,29,39]. Here we show how the set of coupled equations can be solved explicitly at generic frequency and wave vector to obtain the two coupled plasma modes provided by Eq. (35).

We consider a SC system in the absence of external sources, i.e., $\rho_{\rm ext} = 0$ and $\mathbf{J}_{\rm ext} = \mathbf{0}$. The superfluid behavior of the system can be described by means of the first London equation [58], which relates the internal current $\mathbf{J}_{\rm int}$ to the internal electric field $\mathbf{E}$ in a superconductor:

$$\frac{\partial\mathbf{J}_{\rm int}}{\partial t} = e^2 n_s\hat{m}^{-1}\mathbf{E}, \tag{B1}$$

where $\hat{m}$ is the effective mass tensor. In isotropic systems, it trivially reduces to the scalar effective mass m along an arbitrary direction; on the other hand, in anisotropic systems it reads

$$\hat{m} = \begin{pmatrix} m_{xy} & 0 & 0 \\ 0 & m_{xy} & 0 \\ 0 & 0 & m_z \end{pmatrix},$$

where m_{xy} and m_z are the in-plane and the out-of-plane effective masses, respectively.

As is usually done within the mathematical description of e.m. waves, we take the time derivative of both sides of the Biot-Savart law and then substitute Faraday's law, which yields the following equation for the electric field [59]:

$$\nabla^2\mathbf{E} - \boldsymbol{\nabla}(\boldsymbol{\nabla}\cdot\mathbf{E}) = \frac{\varepsilon}{c^2}\frac{\partial^2\mathbf{E}}{\partial t^2} - \frac{4\pi}{c^2}\frac{\partial\mathbf{J}_{\rm int}}{\partial t}. \tag{B2}$$

We can now get rid of $\mathbf{J}_{\rm int}$ by using Eq. (B1) to obtain an equation for the electric field only. Let us introduce the longitudinal $\mathbf{E}_L = (\hat{\mathbf{k}}\cdot\mathbf{E})\hat{\mathbf{k}}$ and the transverse $\mathbf{E}_T = \mathbf{E} - \mathbf{E}_L = (\hat{\mathbf{k}}\times\mathbf{E})\times\hat{\mathbf{k}}$ components of the electric field. In the isotropic case, the

longitudinal-transverse decomposition $\mathbf{E} = \mathbf{E}_L + \mathbf{E}_T$ of the total electric field leads to two decoupled equations:

$$\frac{\partial^2 \mathbf{E}_L}{\partial t^2} - \omega_p^2 \mathbf{E}_L = \mathbf{0}, \tag{B3}$$

$$\frac{\partial^2 \mathbf{E}_T}{\partial t^2} - \tilde{c}^2 \nabla^2 \mathbf{E}_T - \omega_p^2 \mathbf{E}_T = \mathbf{0}, \tag{B4}$$

where the renormalized light velocity is defined as $\tilde{c} = c/\sqrt{\varepsilon}$ as in the main text. In full analogy with Eq. (25), they describe a longitudinal mode oscillating at $\omega = \omega_p$ and two degenerate transverse modes propagating at $\omega^2 = \omega_p^2 + \tilde{c}^2|\mathbf{k}|^2$, ω_p being the isotropic plasma frequency defined in Eq. (16). In the anisotropic case, such a decomposition for the electric field does not decouple the two equations. The main physical reason is that, due to the tensorial nature of the inverse mass tensor, the induced current $\mathbf{J}_{\text{int}}$ in Eq. (B1) is no more parallel to the electric field. Let $\hat{x}$ be, as in the main text, the versor parallel to the direction of the in-plane component of the momentum $\mathbf{k}$. For an anisotropic system, Eq. (B2) splits into three equations. One of them describes the in-plane pure transverse component $\mathbf{E}_T^y = (\hat{\mathbf{y}} \cdot \mathbf{E})\hat{\mathbf{y}}$, which reads

$$\left(\omega^2 - \omega_{xy}^2 - \tilde{c}^2|\mathbf{k}|^2\right)\mathbf{E}_T^y = 0. \tag{B5}$$

In full analogy with the behavior of the ψ_y component of the g.i. phase in Eq. (33), such a transverse mode, which is polarized along the xy plane, is not affected by the anisotropy along the out-of-plane direction, so it propagates without coupling with the longitudinal degrees of freedom. On the other hand, the two equations describing the longitudinal mode $\mathbf{E}_L$ and the transverse component $\mathbf{E}_T^{xz} = (\hat{\mathbf{y}} \times \mathbf{E}) \times \hat{\mathbf{y}} = E_T^{xz}(\hat{\mathbf{k}} \times \hat{\mathbf{y}})$ polarized along the xz plane are coupled. Such equations read, in Fourier space:

$$\begin{aligned}
&\left(\omega^2 - \omega_{xy}^2 \frac{k_x^2}{|\mathbf{k}|^2} - \omega_z^2 \frac{k_z^2}{|\mathbf{k}|^2}\right) E_L \\
&\quad + \frac{k_x k_z}{|\mathbf{k}|^2}\left(\omega_{xy}^2 - \omega_z^2\right) E_T^{xz} = 0, \\
&\left(\omega^2 - \omega_z^2 \frac{k_x^2}{|\mathbf{k}|^2} - \omega_{xy}^2 \frac{k_z^2}{|\mathbf{k}|^2} - \tilde{c}^2|\mathbf{k}|^2\right) E_T^{xz} \\
&\quad + \frac{k_x k_z}{|\mathbf{k}|^2}\left(\omega_{xy}^2 - \omega_z^2\right) E_L = 0.
\end{aligned} \tag{B6}$$

The nontrivial propagating solutions of the previous equations are provided by same the solution of the characteristic polynomial Eq. (34) obtained from the effective action Eq. (33), leading to the frequencies $\omega_\pm$ introduced above. The electric fields $\mathbf{E}_\pm$ associated with such modes can be then computed: One finds that, at leading order in $\mathbf{k}$, they are given exactly by Eq. (43) of the main text, while at generic momentum they are provided by the general decomposition Eq. (44) in longitudinal and transverse components. Note that if the coupling terms $\frac{k_x k_z}{|\mathbf{k}|^2}(\omega_{xy}^2 - \omega_z^2)E_T^{xz}$ and $\frac{k_x k_z}{|\mathbf{k}|^2}(\omega_{xy}^2 - \omega_z^2)E_L$ are neglected in both equations [this is a suitable approximation in the non-relativistic regime Eq. (38)], the pure longitudinal and transverse standard RPA modes ω_L and ω_T are recovered.

Lastly, we remark that Eqs. (B6) can be recast in a form more similar to the one suggested by the action Eq. (33) of the main text, which is $\hat{D}(q)\mathbf{E}(q) = \mathbf{0}$, where the dynamical matrix $\hat{D}$ is defined as follows:

$$\hat{D}(q) \equiv \begin{pmatrix} \omega^2 - \omega_{xy}^2 - \tilde{c}^2 k_z^2 & 0 & \tilde{c}^2 k_x k_z \\ 0 & \omega^2 - \omega_{xy}^2 - \tilde{c}^2|\mathbf{k}|^2 & 0 \\ \tilde{c}^2 k_x k_z & 0 & \omega^2 - \omega_z^2 - \tilde{c}^2 k_x^2 \end{pmatrix}. \tag{B7}$$

By using the latter form, the propagating solutions come from the nontriviality condition for the dynamical matrix $\mathrm{Det}(\hat{D}(q)) = 0$. Note that the matrix $\hat{D}(q)$ and the one associated with Eqs. (B5) and (B6) carry the same information but in two different basis, respectively, the standard cartesian basis and the one spanned by the vectors $\hat{\mathbf{k}}$, $\hat{\mathbf{y}}$ and $\hat{\mathbf{k}} \times \hat{\mathbf{y}}$. The rotation matrix among the two basis reads $\hat{U}(q) = \frac{1}{|\mathbf{k}|}\begin{pmatrix} k_x & 0 & k_z \\ 0 & 1 & 0 \\ -k_z & 0 & k_x \end{pmatrix}$. As a consequence, the 3×3 matrix associated with Eqs. (B5) and (B6) can be trivially computed as $\hat{U}\hat{D}\hat{U}^T$.

[1] S. A. Maier, *Plasmonics: Fundamentals and Applications*, Vol. 1 (Springer, New York, NY, 2007).

[2] P. Nozieres and D. Pines, *Theory Of Quantum Liquids*, Advanced Books Classics (Avalon Publishing, New York, NY, 1999).

[3] A. L. Fetter and J. D. Walecka, *Quantum Theory of Many-Particle Systems* (McGraw-Hill, Boston, 1971).

[4] T. Low, A. Chaves, J. D. Caldwell, A. Kumar, N. X. Fang, P. Avouris, T. F. Heinz, F. Guinea, L. Martin-Moreno, and F. Koppens, Polaritons in layered two-dimensional materials, Nat. Mater. **16**, 182 (2017).

[5] D. N. Basov, M. M. Fogler, and F. J. G. de Abajo, Polaritons in van der Waals materials, Science **354**, aag1992 (2016).

[6] N. Nagaosa and S. Heusler, *Quantum Field Theory in Condensed Matter Physics*, Texts and Monographs in Physics (Springer, New York, NY, 1999).

[7] P. W. Anderson, Random-phase approximation in the theory of superconductivity, Phys. Rev. **112**, 1900 (1958).

[8] I. J. R. Aitchison, P. Ao, D. J. Thouless, and X.-M. Zhu, Effective lagrangians for bcs superconductors at t = 0, Phys. Rev. B **51**, 6531 (1995).

[9] S. De Palo, C. Castellani, C. Di Castro, and B. K. Chakraverty, Effective action for superconductors and BCS-Bose crossover, Phys. Rev. B **60**, 564 (1999).

[10] A. Paramekanti, M. Randeria, T. V. Ramakrishnan, and S. S. Mandal, Effective actions and phase fluctuations in d-wave superconductors, Phys. Rev. B **62**, 6786 (2000).

[11] L. Benfatto, S. Caprara, C. Castellani, A. Paramekanti, and M. Randeria, Phase fluctuations, dissipation, and superfluid stiffness in d-wave superconductors, Phys. Rev. B **63**, 174513 (2001).

[12] L. Benfatto, A. Toschi, and S. Caprara, Low-energy phase-only action in a superconductor: A comparison with the XY model, Phys. Rev. B **69**, 184510 (2004).

[13] Z. Sun, M. M. Fogler, D. N. Basov, and A. J. Millis, Collective modes and terahertz near-field response of superconductors, Phys. Rev. Res. **2**, 023413 (2020).

[14] S. Savel'ev, V. A. Yampol'skii, A. L. Rakhmanov, and F. Nori, Terahertz Josephson plasma waves in layered superconductors: Spectrum, generation, nonlinear and quantum phenomena, Rep. Prog. Phys. **73**, 026501 (2010).

[15] Y. Laplace and A. Cavalleri, Josephson plasmonics in layered superconductors, Adv. Phys.: X **1**, 387 (2016).

[16] B. Keimer, S. A. Kivelson, M. R. Norman, S. Uchida, and J. Zaanen, From quantum matter to high-temperature superconductivity in copper oxides, Nature (London) **518**, 179 (2015).

[17] T. Shibauchi, H. Kitano, K. Uchinokura, A. Maeda, T. Kimura, and K. Kishio, Anisotropic Penetration Depth in $La_{2-x}Sr_xCuO_4$, Phys. Rev. Lett. **72**, 2263 (1994).

[18] C. Panagopoulos, J. R. Cooper, G. B. Peacock, I. Gameson, P. P. Edwards, W. Schmidbauer, and J. W. Hodby, Anisotropic magnetic penetration depth of grain-aligned $HgBa_2Ca_2Cu_3O_{8+\delta}$, Phys. Rev. B **53**, R2999 (1996).

[19] A. Hosseini, D. M. Broun, D. E. Sheehy, T. P. Davis, M. Franz, W. N. Hardy, R. Liang, and D. A. Bonn, Survival of the d-Wave Superconducting State Near the Edge of Antiferromagnetism in the Cuprate Phase Diagram, Phys. Rev. Lett. **93**, 107003 (2004).

[20] D. van der Marel and A. Tsvetkov, Transverse optical plasmons in layered superconductors, Czech. J. Phys. **46**, 3165 (1996).

[21] K. Tamasaku, Y. Nakamura, and S. Uchida, Charge Dynamics Across the CuO_2 Planes in $La_{2-x}Sr_xCuO_4$, Phys. Rev. Lett. **69**, 1455 (1992).

[22] C. C. Homes, T. Timusk, R. Liang, D. A. Bonn, and W. N. Hardy, Optical Conductivity of C Axis Oriented $YBa_2Cu_3O_{6.70}$: Evidence for a Pseudogap, Phys. Rev. Lett. **71**, 1645 (1993).

[23] J. H. Kim, H. Somal, M. Czyzyk, D. van der Marel, A. Wittlin, A. Gerrits, V. Duijn, N. Hien, and A. Menovsky, Strong damping of the c-axis plasmon in high-Tc cuprate superconductors, Physica C **247**, 297 (1995).

[24] D. N. Basov, T. Timusk, B. Dabrowski, and J. D. Jorgensen, c-axis response of $YBa_2Cu_4O_8$: A pseudogap and possibility of josephson coupling of CuO_2 planes, Phys. Rev. B **50**, 3511 (1994).

[25] M. Machida, T. Koyama, and M. Tachiki, Dynamical breaking of charge neutrality in intrinsic Josephson junctions: Common origin for microwave resonant absorptions and multiple-branch structures in the $I-V$ characteristics, Phys. Rev. Lett. **83**, 4618 (1999).

[26] M. Machida, T. Koyama, A. Tanaka, and M. Tachiki, Theory of the superconducting phase and charge dynamics in intrinsic Josephson-junction systems: Microscopic foundation for longitudinal Josephson plasma and phenomenological dynamical equations, Physica C **331**, 85 (2000).

[27] C. Helm and L. N. Bulaevskii, Optical properties of layered superconductors near the Josephson plasma resonance, Phys. Rev. B **66**, 094514 (2002).

[28] S. Savel'ev, A. L. Rakhmanov, V. A. Yampol'skii, and F. Nori, Analogues of nonlinear optics using terahertz Josephson plasma waves in layered superconductors, Nat. Phys. **2**, 521 (2006).

[29] L. N. Bulaevskii, M. Zamora, D. Baeriswyl, H. Beck, and J. R. Clem, Time-dependent equations for phase differences and a collective mode in Josephson-coupled layered superconductors, Phys. Rev. B **50**, 12831 (1994).

[30] A. Bill, H. Morawitz, and V. Z. Kresin, Electronic collective modes and superconductivity in layered conductors, Phys. Rev. B **68**, 144519 (2003).

[31] A. L. Fetter, Electrodynamics of a layered electron gas. II. Periodic array, Ann. Phys. **88**, 1 (1974).

[32] V. Z. Kresin and H. Morawitz, Layer plasmons and high-T_c superconductivity, Phys. Rev. B **37**, 7854 (1988).

[33] R. S. Markiewicz, M. Z. Hasan, and A. Bansil, Acoustic plasmons and doping evolution of Mott physics in resonant inelastic x-ray scattering from cuprate superconductors, Phys. Rev. B **77**, 094518 (2008).

[34] A. Greco, H. Yamase, and M. Bejas, Origin of high-energy charge excitations observed by resonant inelastic x-ray scattering in cuprate superconductors, Commun. Phys. **2**, 3 (2019).

[35] S. Rajasekaran, E. Casandruc, Y. Laplace, D. Nicoletti, G. D. Gu, S. R. Clark, D. Jaksch, and A. Cavalleri, Parametric amplification of a superconducting plasma wave, Nat. Phys. **12**, 1012 (2016).

[36] S. Rajasekaran, J. Okamoto, L. Mathey, M. Fechner, V. Thampy, G. D. Gu, and A. Cavalleri, Probing optically silent superfluid stripes in cuprates, Science **359**, 575 (2018).

[37] K. A. Cremin, J. Zhang, C. C. Homes, G. D. Gu, Z. Sun, M. M. Fogler, A. J. Millis, D. N. Basov, and R. D. Averitt, Photoenhanced metastable c-axis electrodynamics in stripe-ordered cuprate $La_1.885Ba_0.115CuO_4$, Proc. Natl. Acad. Sci. **116**, 19875 (2019).

[38] D. Fu, D. Nicoletti, M. Fechner, M. Buzzi, and G. D. G. and A. Cavalleri, Phys. Rev. B **105**, L020502 (2022).

[39] M. H. Michael, A. von Hoegen, M. Fechner, M. Först, A. Cavalleri, and E. Demler, Parametric resonance of Josephson plasma waves: A theory for optically amplified interlayer superconductivity in $YBa_2Cu_3O_{6+x}$, Phys. Rev. B **102**, 174505 (2020).

[40] F. Gabriele, M. Udina, and L. Benfatto, Non-linear terahertz driving of plasma waves in layered cuprates, Nat. Commun. **12**, 752 (2021).

[41] P. E. D. *et al.*, Periodic dynamics in superconductors induced by an impulsive optical quench, arXiv:2104.07181.

[42] H. T. Stinson, J. S. Wu, B. Y. Jiang, Z. Fei, A. S. Rodin, B. C. Chapler, A. S. McLeod, A. Castro Neto, Y. S. Lee, M. M. Fogler, and D. N. Basov, Infrared nanospectroscopy and imaging of collective superfluid excitations in anisotropic superconductors, Phys. Rev. B **90**, 014502 (2014).

[43] Q. Lu, A. T. Bollinger, X. He, R. Sundling, I. Bozovic, and A. Gozar, Surface Josephson plasma waves in a

high-temperature superconductor, npj Quantum Mater. **5**, 69 (2020).

[44] F. J. García de Abajo, Optical excitations in electron microscopy, Rev. Mod. Phys. **82**, 209 (2010).

[45] M. Hepting, L. Chaix, E. W. Huang, R. Fumagalli, Y. Y. Peng, B. Moritz, K. Kummer, N. B. Brookes, W. C. Lee, M. Hashimoto, T. Sarkar, J. F. He, C. R. Rotundu, Y. S. Lee, R. L. Greene, L. Braicovich, G. Ghiringhelli, Z. X. Shen, T. P. Devereaux, and W. S. Lee, Three-dimensional collective charge excitations in electron-doped copper oxide superconductors, Nature (London) **563**, 374 (2018).

[46] J. Lin, J. Yuan, K. Jin, Z. Yin, G. Li, K.-J. Zhou, X. Lu, M. Dantz, T. Schmitt, H. Ding, H. Guo, M. P. M. Dean, and X. Liu, Doping evolution of the charge excitations and electron correlations in electron-doped superconducting $La_{2-x}Ce_xCuO_4$, npj Quantum Mater. **5**, 4 (2020).

[47] A. Nag, M. Zhu, M. Bejas, J. Li, H. C. Robarts, H. Yamase, A. N. Petsch, D. Song, H. Eisaki, A. C. Walters, M. García-Fernández, A. Greco, S. M. Hayden, and K.-J. Zhou, Detection of Acoustic Plasmons in Hole-Doped Lanthanum and Bismuth Cuprate Superconductors using Resonant Inelastic x-Ray Scattering, Phys. Rev. Lett. **125**, 257002 (2020).

[48] M. Mitrano, A. A. Husain, S. Vig, A. Kogar, M. S. Rak, S. I. Rubeck, J. Schmalian, B. Uchoa, J. Schneeloch, R. Zhong, G. D. Gu, and P. Abbamonte, Anomalous density fluctuations in a strange metal, Proc. Natl. Acad. Sci. **115**, 5392 (2018).

[49] A. A. Husain, M. Mitrano, M. S. Rak, S. Rubeck, B. Uchoa, K. March, C. Dwyer, J. Schneeloch, R. Zhong, G. D. Gu, and P. Abbamonte, Crossover of Charge Fluctuations Across the Strange Metal Phase Diagram, Phys. Rev. X **9**, 041062 (2019).

[50] J. Fink, Comment on: Crossover of charge fluctuations across the strange metal phase diagram, arXiv:2103.10268.

[51] A. Husain, M. Mitrano, A., M. S. Rak, S. I. Rubeck, B. Uchoa, K. March, C. Dwyer, J. Schneeloch, R. Zhong, G. D. Gu, and P. Abbamonte, arXiv:2106.03301.

[52] P. W. Anderson, Plasmons, gauge invariance, and mass, Phys. Rev. **130**, 439 (1963).

[53] P. Konsin and B. Sorkin, Electric field effects in high-T_c cuprates, Phys. Rev. B **58**, 5795 (1998).

[54] Z. Sun, Á. Gutiérrez-Rubio, D. N. Basov, and M. M. Fogler, Hamiltonian optics of hyperbolic polaritons in nanogranules, Nano Letters, Nano Lett. **15**, 4455 (2015).

[55] A. Poddubny, I. Iorsh, P. Belov, and Y. Kivshar, Hyperbolic metamaterials, Nat. Photonics **7**, 948 (2013).

[56] R. Senga, K. Suenaga, P. Barone, S. Morishita, F. Mauri, and T. Pichler, Position and momentum mapping of vibrations in graphene nanostructures, Nature (London) **573**, 247 (2019).

[57] N. Li, X. Guo, X. Yang, R. Qi, T. Qiao, Y. Li, R. Shi, Y. Li, K. Liu, Z. Xu, L. Liu, F. J. García de Abajo, Q. Dai, E.-G. Wang, and P. Gao, Direct observation of highly confined phonon polaritons in suspended monolayer hexagonal boron nitride, Nat. Mater. **20**, 43 (2021).

[58] M. Tinkham, *Introduction to Superconductivity* (Courier Corporation, 2004).

[59] D. J. Griffiths, Introduction to electrodynamics (2005).